

# Locally Adaptive Random Walk Stochastic Volatility

Jason B. Cho\*

Department of Statistics and Data Science, Cornell University  
and

David S. Matteson

Department of Statistics and Data Science, Cornell University

August 22, 2024

## Abstract

We introduce a novel Bayesian framework for estimating time-varying volatility by extending the Random Walk Stochastic Volatility (RWSV) model with a new Dynamic Shrinkage Process (DSP) in (log) variances. Unlike classical Stochastic Volatility or GARCH-type models with restrictive parametric stationarity assumptions, our proposed Adaptive Stochastic Volatility (ASV) model provides smooth yet dynamically adaptive estimates of evolving volatility and its uncertainty (vol of vol). We derive the theoretical properties of the proposed global-local shrinkage prior. Through simulation studies, we demonstrate that ASV exhibits remarkable misspecification resilience with low prediction error across various data generating scenarios in simulation. Furthermore, ASV's capacity to yield locally smooth and interpretable estimates facilitates a clearer understanding of underlying patterns and trends in volatility. Additionally, we propose and illustrate an extension for Bayesian Trend Filtering simultaneously in both mean and variance. Finally, we show that this attribute makes ASV a robust tool applicable across a wide range of disciplines, including in finance, environmental science, epidemiology, and medicine, among others.

*Keywords:* Time series; Trend filtering; Dynamic linear model;

---

\*The authors gratefully acknowledge financial support from *National Science Foundation grants OAC-1940124 and DMS-2114143*

# 1 Introduction

Volatility in a time series indicates how much the series deviates from its average value. Estimating volatility holds significant importance across diverse fields as it offers crucial insights into the underlying data generation process. In finance, for instance, understanding the volatility of financial assets is pivotal for derivative pricing, asset valuation, portfolio management, and overall risk assessment. In epidemiology, estimating the volatility of new disease cases enables early detection of major outbreaks (Kostoulas et al. [2021]) and enhances predictions of number of new cases (Achcar et al. [2020], Sarkar and Chatterjee [2017]). Climate scientists utilize time-varying volatility models to analyze various climate phenomena like tornadoes (Tippett [2014]), droughts (Modarres and Ouarda [2014]), and rainfall patterns (Mehdizadeh et al. [2017]). Similarly, in mechanical systems, volatility estimates derived from acceleration envelope readings aid in predicting machine failures (Pham and Yang [2010], Ma et al. [2017]). Additionally, in hydrology, understanding the volatility of river streamflows, which can vary drastically due to climate change, is achieved through time-varying volatility models (Wang et al. [2005, 2023a,b], Otache [2012]).

Commonly studied statistical models for estimating time-varying volatility include the Autoregressive Conditional Heteroskedasticity (ARCH) model [Engle, 1982], the Generalized ARCH (GARCH) model [Bollerslev, 1986], and the Stochastic Volatility (SV) model [Hull and White, 1987, Taylor, 2008, Melino and Turnbull, 1990]. However, these models, due to their parametric stationarity assumptions, often suffer from model misspecification, leading to inaccurate estimation, especially when the underlying volatility process undergoes gradual or abrupt changes. Unfortunately, such changes are commonplace across various disciplines, rendering volatility estimates from these models unreliable. In finance, empirical studies by Chou [1988], French et al. [1987], Poon and Taylor [1992], So et al.

[1997], Su and Wang [2020] and Nishino and Kakamu [2015] all point to changes in underlying volatility process evidenced by high persistence. Similarly, scientists observe changes in volatility processes during extreme weather events (Tippett [2014]) attributed to climate change. In epidemiology, volatility in the number of new disease cases is expected to change due to seasonal effects or large outbreaks (Kostoulas et al. [2021]). Thus, there is a clear need for a flexible framework capable of adaptively estimating volatility, accommodating both gradual and abrupt changes.

A widely adopted strategy for accommodating changes in the underlying volatility process involves incorporating time-varying parameters into the aforementioned parametric models, thereby enhancing model flexibility. One of the popular methods to model time variation in parameters is via latent Markov switching models [Brunetti et al., 2008, Ardia et al., 2018, Caporale and Zekokh, 2019, Sajjad et al., 2008, Dueker, 1997]. Under this framework, parameters are time-varying and are assumed to originate from a fixed number of latent regimes, with transitions between regimes governed by a hidden Markov process. The inclusion of multiple regimes allows for greater flexibility compared to single-regime models. However, determining the number of latent regimes *a priori* remains a challenge. Additionally, estimating the latent regime at each time point as well as the transition probabilities between regimes adds to the complexity of parameter estimation. Note that the number of transition probabilities to be estimated grow quadratically with the number of regimes. Latent regime switching framework has been integrated into aforementioned parametric models such as the Markov-Switching ARCH by Hamilton and Susmel [1994] and Cai [1994], the Markov-Switching GARCH model by Bauwens et al. [2010] and Gray [1996], and the Markov-Switching SV model by So et al. [1998] and Hwang et al. [2004].

Herein, we present the Adaptive Stochastic Volatility (ASV) model, building upon the

Random Walk Stochastic Volatility (RWSV) model explored in Ruiz [1994] and Harvey et al. [1994]. RWSV commonly assumes the log-variance of the observed process follows a Gaussian random walk with a constant variance. In contrast, ASV introduces two significant modifications to RWSV: it incorporates a time-varying variance for the log-variance increments and adopts a global-local shrinkage prior for adaptability.

ASV’s local adaptability is a standout feature, effectively estimating volatility in the presence of gradual or abrupt changes in the volatility process with notable smoothness in between. It allows robustness against model misspecification, resulting in low prediction errors across diverse data-generating scenarios. In addition, ASV’s volatility estimates exhibit smoother trajectories compared to those generated by alternative time-varying parameter models. The reduction in noise within our estimates provides users with clearer insights into underlying patterns and trends in the data. We also propose an intermediary model, RWSV with a time-varying shrinkage prior but without the global-local structure, called RWSV with Bayesian LASSO (RWSV-BL). However, our results suggest that this model undersmooths and performs similarly to RWSV in most cases.

We specifically highlight a class of global-local shrinkage prior called Dynamic Shrinkage Processes (DSP) [Kowal et al., 2019], which includes dynamic versions of a horseshoe prior [Carvalho et al., 2010] as a special case. DSP has shown versatility across various applications. For example, Wu et al. [2024a] integrates DSP into a Bayesian dynamic linear model to estimate change points and score outliers. Another application is seen in Schafer and Matteson, where DSP is used to propose the negative binomial Bayesian trend filter (NB-BTF) for adaptively smoothing integer-valued time series. Additionally, Wu et al. [2024b] combines the Bayesian trend filter with DSP and machine learning-based regularization method to effectively distinguish micro-level drifts from macro-level shifts.

Kowal et al. [2019] has also shown superior performance for trend filtering when compared against other shrinkage priors. DSP has been applied in the context of Stochastic Volatility in Mean (SVM) modeling [Huber and Pfarrhofer, 2021], where DSP is imposed on its time-varying regression on variance within the conditional mean of the process.

Section 2 introduces the model and its associated parameters; theoretical properties of DSP in comparison to other shrinkage priors are explored. Section 3 provides an overview of the Gibbs sampling scheme; Full conditional distributions are detailed in the supplementary material. Comparisons between proposed models on simulated data are presented in Section 4. Subsequently, Section 5 presents empirical analyses of three datasets: weekly log-returns on the S&P 500 index, weekly log-returns on EURO/USD exchange rate and weekly changes in death tolls from COVID-19 in the U.S. based on the proposed method. In Section 6, We propose Bayesian Trend Filter with Adaptive Stochastic Volatility (BTF-ASV) combining Bayesian Trend Filter with Dynamic Horseshoe Process (BTF-DHP) by Kowal et al. [2019] and Adaptive Stochastic Volatility model (ASV) proposed in this paper for simultaneously estimating both the time-varying means and the variances. The model is then applied to the surface air temperature anomaly data for empirical analysis.

## 2 Methodology

### 2.1 The Random Walk Stochastic Volatility Model

Our method, Adaptive Stochastic Volatility (ASV), may be thought of as an extension of Random Walk Stochastic Volatility (RWSV) model explored in Ruiz [1994] and Harvey et al. [1994]. Consider a zero mean process with  $T$  observations,  $\{y_t\}_{t=1}^T$ , and its log-variance term  $\{h_t\}_{t=1}^T$ . Stochastic Volatility (SV) model assumes the observed process  $y_t$  to follow a normal distribution with its log-variance term,  $h_t$ , following the lag order 1 autoregression. RWSV is a special case of SV model where the autoregressive coefficient is assumed to be

1. Thus, the model is defined as:

$$y_t = \exp\{h_t/2\}\epsilon_t \quad \epsilon_t \stackrel{iid}{\sim} N(0, 1)$$

$$\Delta h_t := h_t - h_{t-1} = \sigma_h u_t \quad u_t \stackrel{iid}{\sim} N(0, 1).$$

Unlike the SV model, RWSV is a unit-root non-stationary process. This assumption is substantiated by financial asset return analyses, as evidenced by several studies, including Chou [1988], French et al. [1987], Poon and Taylor [1992], So et al. [1997], Su and Wang [2020] and Nishino and Kakamu [2015], which consistently find that the autoregressive coefficient of the SV model fitted to stock market returns is close to 1. In RWSV,  $h_t$  is governed by a time-invariant variance term,  $\sigma_h^2$ , which determines the degree of variation between successive log-variances. A large  $\sigma_h^2$  implies high probability of significant changes in the  $h_t$  process, whereas a small  $\sigma_h^2$  indicates high probability of minimal to no changes in  $h_t$ . In a frequentist framework,  $\sigma_h$  is typically treated as a fixed parameter, often estimated via Quasi-Maximum Likelihood, as demonstrated in the original papers by Ruiz [1994] and Harvey et al. [1994]. More recent studies, such as that by Nishino and Kakamu [2015], have employed a Bayesian framework for estimation with a non-informative prior on  $\sigma_h^2$ .

## 2.2 Stochastic Volatility with Only Local Shrinkage

RWSV model, however, may provide a poor fit for time series exhibiting periods of both significant and minimal changes due to its assumption of a time-invariant  $\sigma_h^2$ . Ideally, we prefer  $\sigma_h^2$  to be time-varying, remaining small during periods of little to no significant changes and increasing to a large value during periods of abrupt changes in  $h_t$ . This problem is akin to high-dimensional regression problem as such model would require the number of parameters to be larger than the number of samples. A common frequentist approach to addressing this problem is by imposing an additional penalty term like the  $l1$  penalty (Tibshirani [1996]). Similarly in Bayesian setting, sparsity inducing priors may be

imposed on the parameters. Drawing from Bayesian representations of LASSO as discussed in Park and Casella [2008] and the scale-mixture Gaussian representation of the Laplace distribution in West [1987], we propose an intermediary model called RWSV with Bayesian LASSO (RWSV-BL), which incorporates a time-varying variance for  $h_t$  as

$$\Delta h_t \sim N(0, \sigma_{h,t}^2) \quad \sigma_{h,t}^2 \stackrel{iid}{\sim} \text{Exp}\{(2\Lambda^2)^{-1}\}.$$

Under this Bayesian representation,  $\Delta h_t$  follows a normal distribution with one time-varying local parameter  $\sigma_{h,t}^2$ . RWSV-BL shares similarities with the  $l1$ -trend filter proposed by Kim et al. [2009] and Tibshirani [2014], which aims to provide a smooth estimate of the observed process  $y_t$ . The key distinction between the  $l1$ -trend filter and RWSV-BL lies in their respective focuses: while the  $l1$ -trend filter targets the estimation of the time-varying mean of the process, RWSV-BL is designed to estimate the time-varying log-variance,  $h_t$  instead. Drawing an analogy between the trend-filter and RWSV-BL allows us to conceptualize our problem as a smoothing task applied to the variance process. By incorporating shrinkage priors on the higher-order differences of the log-variance process, the model can achieve greater smoothing on  $h_t$ .

### 2.3 Adaptive Stochastic Volatility via Global-Local Shrinkage

Building upon the model in the previous subsection, we propose the Adaptive Stochastic Volatility (ASV) model. Unlike RWSV-BL, which consists of a time-varying local parameter, ASV features a global-local structure for the variance of the log-variance,  $\sigma_{h,t}^2$ . Specifically,  $\sigma_{h,t}$  is defined as  $\sigma_{h,t} := \tau \lambda_t$ , where  $\tau$  represents the global parameter, and  $\lambda_t$  represents the local parameter. The global parameter  $\tau$  controls the overall shrinkage and acts as the average shrinkage applied across all time points, while the local parameter  $\lambda_t$  controls smoothness at each time  $t$  in addition to  $\tau$ . The inclusion of the global parameter  $\tau$  enhances model smoothness by providing a consistent level of shrinkage across all

time points, which we find as essential in the application and simulations sections below. In contrast, the Bayesian LASSO model, as discussed in section 2.2 only incorporates a local parameter for  $\sigma_{h,t}^2$ . Section 5 shows ASV to yield significantly smoother estimates of  $h_t$  compared to RWSV-BL. Therefore, we propose the following model for estimating time-varying volatility:

$$\Delta^k h_t \sim N(0, \tau \lambda_t) \quad \tau \sim \pi(\tau), \quad \lambda_t \stackrel{iid}{\sim} \pi(\lambda_t),$$

where  $k$  is usually set to 1 or 2, and  $\pi(\tau)$  and  $\pi(\lambda_t)$  represent priors on  $\tau$  and  $\lambda_t$ . Global-local shrinkage priors for Gaussian observations have been extensively studied in the past decade, particularly in the context of high-dimensional regression. Examples of such priors include the Horseshoe prior by Carvalho et al. [2010], the Horseshoe plus prior by Bhadra et al. [2015], the triple gamma prior by Cadonna et al. [2019], and Dynamic Shrinkage Processes (DSP) introduced by Kowal et al. [2019]. The global parameter,  $\tau$ , ensures that the estimate of  $h_t$  remains smooth overall, while the local parameter,  $\lambda_t$ , allows for local adaptivity in the presence of abrupt changes. Among the various aforementioned global-local priors, DSP are further analyzed and incorporated into the ASV model in this work. Two versions of ASV are explored: Adaptive Stochastic Volatility with Dynamic Shrinkage Process (ASV-DSP) and Adaptive Stochastic Volatility with Horseshoe Prior (ASV-HP), the latter of which can be considered a special case of ASV-DSP.

## 2.4 Properties of Dynamic Shrinkage Processes

DSP distinguish themselves among global-local priors by incorporating temporal dependence in the local shrinkage parameter  $\lambda_t$ , allowing for a dynamic shrinkage approach. Kowal et al. [2019] applied DSP in Bayesian trend filtering and demonstrated its superior performance in terms of prediction error when estimating the mean of an arbitrary time series, compared to other well-studied horseshoe prior. Therefore, we focus on DSP as the

prior distribution on  $h_t$ . Under this framework,  $h_t \sim N(0, \sigma_{h,t}^2)$  and the priors on  $\sigma_{h,t}$  are defined by its log-squared term,  $v_t := \log(\sigma_{h,t}^2)$ :

$$v_t = \mu + \psi_t + \eta_t \quad \eta_t \stackrel{iid}{\sim} Z(a, b, 0, 1),$$

where  $Z$ -distribution has the following density function (Barndorff-Nielsen et al. [1982]):

$$f(z|a, b, \mu_z, \sigma_z) = (\sigma_z \beta(a, b))^{-1} \left( \exp \left\{ \frac{z - \mu_z}{\sigma_z} \right\} \right)^a \left( 1 + \exp \left\{ \frac{z - \mu_z}{\sigma_z} \right\} \right)^{-(a+b)}.$$

For the global parameter,  $\tau = \exp\{\mu/2\}$  and  $\lambda_t = \exp\{(\psi_t + \eta_t)/2\}$  represents the local parameter. Specifically,  $\psi_t$  models the temporal dependence of the process. A few candidate models for  $\psi_t$  includes the Hidden Markov Models, linear regression, or spline. For simplicity, the serial dependence is assumed to be positive, indicating that large  $\sigma_{h,t}^2$  is likely to result in large  $\sigma_{h,t+1}^2$ . Heuristic interpretation of this assumption is that large changes is likely to be followed by another large changes, while small changes is likely to be followed by small changes. Thus,  $\psi_t := \phi(v_t - \mu)$ , with  $\eta_t \sim Z(a, b, 0, 1)$  corresponding to the i.i.d scale parameter. The benefit of having  $Z$ -distribution as prior on  $\eta_t$  is its shrinkage property. By setting  $a = b = 1/2$  and  $\phi = 0$ , we have the horseshoe prior (Carvalho et al. [2010]), as  $\lambda_t = \exp\{\eta_t/2\} \sim C^+(0, 1)$  is equivalent to  $\eta_t \sim Z(1/2, 1/2, 0, 1)$ .

Owing to its autoregressive structure, the shrinkage profile of DSP is analyzed conditional on either the previous shrinkage term  $\kappa_t := \frac{1}{1+\exp\{v_t\}}$  or the local scale parameter  $\lambda_t$ , which both follow Three Parameter Beta distribution (Kowal et al. [2019]). We consider the shrinkage profile of the stationary distribution of  $v_t$ . We show that DSP has similar properties as Horseshoe prior but induces heavier shrinkage. Let's first define  $z_{t,h} := \phi^h \eta_{t-h}$ .

Infinite order Moving Average representation of  $v_t$  results in:

$$\begin{aligned}
v_t &= \mu + \phi(v_{t-1} - \mu) + \eta_t & \eta_t \sim Z(1/2, 1/2, 0, 1) \\
&= \mu + \sum_{h=0}^{\infty} \phi^h \eta_{t-h} \\
&= \mu + \sum_{h=0}^{\infty} z_{t,h}.
\end{aligned}$$

As shown in Barndorff-Nielsen et al. [1982],  $z_{t,h}$  is a scaled Hyperbolic Secant Distribution, with  $E(z_{t,h}|\phi) = 0$  and  $Var(z_{t,h}|\phi) = (|\phi|^h \pi)^2$ . Let's consider  $z_t := \sum_{h=0}^{\infty} z_{t,h}$ .

**Theorem 1.**  $z_t$  converges almost surely if and only if  $|\phi| < 1$ .

*Proof.* This directly follows from Kolmogorov's three series theorem. Note that the variance  $\sum_{h=0}^{\infty} var(z_{t,h}|\phi)$  converges if and only if  $|\phi| < 1$ . Exact derivation is explored in Appendix A.1.  $\square$

**Corollary 1.1.** When  $|\phi| < 1$ ,

$$\begin{aligned}
E(z_t|\phi) &= E\left(\sum_{h=0}^{\infty} z_{t,h}|\phi\right) = \sum_{h=0}^{\infty} E(z_{t,h}|\phi) = 0 \\
var(z_t|\phi) &= var\left(\sum_{h=0}^{\infty} z_{t,h}|\phi\right) = \sum_{h=0}^{\infty} var(z_{t,h}|\phi) = \sum_{h=0}^{\infty} \pi^2 \phi^{2h} = \frac{\pi^2}{1 - \phi^2}
\end{aligned}$$

Characteristic function of  $z_{h,t}$  is  $sech(\pi\phi^h t)$ . Thus, the characteristic function,  $g(t)$ , for  $\sum_{h=0}^{\infty} z_{h,t}$ , would be an infinite product of the characteristic function of  $z_{h,t}$ .

$$g(t) = \prod_{h=0}^{\infty} sech(\pi\phi^h t) \quad -\frac{1}{2} < t < \frac{1}{2}$$

Similarly, for the Moment Generating function  $M(t)$

$$M(t) = \prod_{h=0}^{\infty} sec(\pi\phi^h t) = \prod_{h=0}^{\infty} \frac{1}{cos(\pi\phi^h t)}, \quad -\frac{1}{2} < t < \frac{1}{2}$$

**Theorem 2.** If  $|\phi| = 0.5$ ,  $\eta_{t-h} \stackrel{iid}{\sim} Z(1/2, 1/2, 0, 1)$ , and  $z_{t,h} := \phi^h \eta_{t-h}$ , then  $z_t := \sum_{h=0}^{\infty} z_{t,h} \xrightarrow{a.s.} Logistic(0, 2)$ .

*Proof.* Derivations are explored in Appendix A.2.  $\square$

Thus, assuming  $\mu = 0$  and  $\phi = 0.5$  for simplicity, we have the following density function

for  $v_t$ ,  $\lambda_t := \exp\{v_t/2\}$  and  $\kappa_t := \frac{1}{1+\exp\{v_t\}}$  for the stationary distribution of DSP:

$$f(v_t) = \frac{1}{8} \operatorname{sech}^2\left(\frac{v_t}{4}\right)$$

$$f(\lambda_t) = \frac{1}{4\lambda_t} \operatorname{sech}^2\left(\frac{\log(\lambda_t)}{2}\right) = \frac{1}{(1+\lambda_t)^2}$$

$$f(\kappa_t) = \frac{1}{8(\kappa_t)(1-\kappa_t)} \operatorname{sech}^2\left(\frac{1}{4}\left(\log\left(\frac{1-\kappa_t}{\kappa_t}\right)\right)\right) = \frac{1}{\sqrt{\kappa_t(1-\kappa_t)}} \frac{1}{2\kappa_t(1+\sqrt{\frac{1-\kappa_t}{\kappa_t}})^2}.$$

Figure 2.4 compares the prior distribution of  $\lambda_t$  and  $\kappa_t$  for the Horseshoe and DSP. Let's

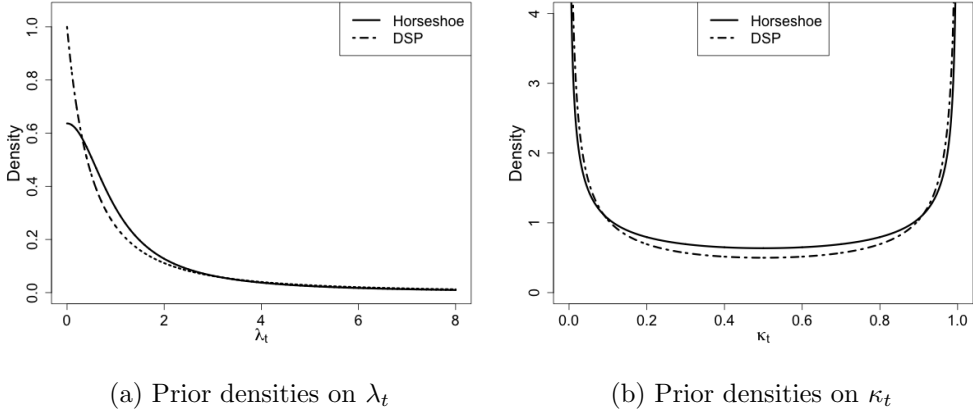


Figure 1: Comparisons of prior densities on  $\lambda_t$  and  $\kappa_t$  between Horseshoe Prior and the stationary distribution of Dynamic Shrinkage Process (DSP) with  $\eta_t \stackrel{iid}{\sim} Z(1/2, 1/2, 0, 1)$ ,  $\phi = 1/2$  and  $\mu = 0$ .

remind ourselves that the Horseshoe prior in Carvalho et al. [2010] assumes  $\lambda_t \sim C^+(0, 1)$

and  $\kappa_t \sim \text{Beta}(1/2, 1/2)$ . The density function for Horseshoe,  $g(\lambda_t)$  and  $g(\kappa_t)$  are:

$$g(\lambda_t) = \frac{2}{\pi(1+\lambda_t^2)} \quad g(\kappa_t) = \frac{1}{\pi\sqrt{\kappa_t(1-\kappa_t)}}.$$

For  $\lambda_t$ , the density function for DSP puts more weights as  $\lambda_t \rightarrow 0$  and  $\lambda_t \rightarrow \infty$ . Specifically,

$f(\lambda_t) > g(\lambda_t)$  when  $\lambda_t \in (0, \frac{2-\sqrt{(4-\pi)\pi}}{(\pi-2)}) \cup (\frac{2+\sqrt{(4-\pi)\pi}}{(\pi-2)}, \infty)$ . In terms of  $\kappa_t$ , the DSP puts

more weight around 0 and 1 than Horseshoe. This is due to the extra U-shaped term in

$\kappa_t$ ,  $\frac{1}{2\kappa_t(1+\sqrt{\frac{1-\kappa_t}{\kappa_t}})^2}$ , pushing the mass of the distribution to near 0 and 1. Let's consider the marginal density on  $\Delta h$ .

**Theorem 3.** Let  $|\phi| = 0.5$ ,  $\eta_{t-h} \stackrel{iid}{\sim} Z(1/2, 1/2, 0, 1)$ ,  $z_{t,h} := \phi^h \eta_{t-h}$ ,  $v_t := \sum_{h=0}^{\infty} z_{t,h}$ ,  $\lambda_t :=$

$\exp\{v_t/2\}$  and  $\Delta h_t \sim N(0, \lambda_t)$ ,

$$\lim_{\Delta h_t \rightarrow 0} f(\Delta h_t) = \infty$$

$$K_L \log\left(1 + \frac{4}{\Delta^2 h_t}\right) < f(\Delta h_t) < K_U \log\left(1 + \frac{2}{\Delta^2 h_t}\right), \quad |\Delta h_t| > 0$$

where  $K_U = \frac{1}{2\sqrt{2\pi}}$  and  $K_L = \frac{1}{8\sqrt{2\pi}}$

*Proof.* The proof is similar to Theorem 1 in Carvalho et al. [2010]. We use the fact that

$\forall x > 0$ ,

$$\frac{1}{2(1+x^2)} \leq \frac{1}{(1+x)^2} \leq \frac{1}{(1+x^2)}$$

Derivation is detailed in Appendix A.3.  $\square$

The bounds for the marginal distribution of DSP are similar to the ones from the Horseshoe with the only difference being the constant factor  $K_L$  and  $K_U$ . Under Horseshoe,  $K_U = \frac{1}{\sqrt{2\pi^3}}$  and  $K_L = \frac{1}{2\sqrt{2\pi^3}}$ . Like horseshoe prior, DSP is also unbounded near the origin, which leads to super-efficiency in a sparse setting as shown in Carvalho et al. [2010].

## 2.5 Jointly Modeling Both Trends in Mean and Variance

Finally, we propose Bayesian Trend Filter with Adaptive Stochastic Volatility (BTF-ASV) by combining Bayesian Trend Filter with Dynamic Horseshoe Process (BTF-DHP) proposed in Kowal et al. [2019] and ASV model proposed in this paper. BTF-ASV is able to generate smooth and locally adaptive estimate of the time varying mean parameter  $\beta_t$  through the Bayesian Trend Filter, and the time varying log variance parameter  $h_t$  via ASV, simultaneously.

Let's define  $\omega_{\beta,t} := \Delta^k \beta_t$  and also similarly define for variables  $v_{\beta,t}, u_{\beta,t}, \mu_{\beta}, \phi_{\beta}, \eta_{\beta,t}$  as well as for hyper-parameters  $a_{\eta_{\beta}}, b_{\eta_{\beta}}, a_{\mu_{\beta}}, b_{\mu_{\beta}}, a_{\phi_{\beta}}, b_{\phi_{\beta}}$ . We have the following Bayesian

hierarchical representation of BTF-ASV:

$$y_t = \beta_t + \exp\{h_t/2\}\epsilon_t \quad \epsilon_t \stackrel{iid}{\sim} N(0, 1) \quad (1a)$$

$$\Delta^k \beta_t = \omega_{\beta,t} = \exp\{v_{\beta,t}/2\}u_{\beta,t} \quad u_{\beta,t} \stackrel{iid}{\sim} N(0, 1) \quad (1b)$$

$$v_{\beta,t+1} = \mu_\beta + \phi_\beta(v_{\beta,t} - \mu_\beta) + \eta_{\beta,t} \quad \eta_{\beta,t} \stackrel{iid}{\sim} Z(a_{\eta_\beta}, b_{\eta_\beta}, 0, 1) \quad (1c)$$

$$\mu_h \sim Z(a_{\mu_\beta}, b_{\mu_\beta}, 0, 1) \quad (\phi_\beta + 1)/2 \sim Beta(a_{\phi_\beta}, b_{\phi_\beta}) \quad (1d)$$

$$\Delta^k h_t = \omega_{h,t} = \exp\{v_{h,t}/2\}u_{h,t} \quad u_{h,t} \stackrel{iid}{\sim} N(0, 1) \quad (1e)$$

$$v_{h,t+1} = \mu_h + \phi_h(v_{h,t} - \mu_h) + \eta_{h,t} \quad \eta_{h,t} \stackrel{iid}{\sim} Z(a_{\eta_h}, b_{\eta_h}, 0, 1) \quad (1f)$$

$$\mu_h \sim Z(a_{\mu_h}, b_{\mu_h}, 0, 1) \quad (\phi_h + 1)/2 \sim Beta(a_{\phi_h}, b_{\phi_h}) \quad (1g)$$

Line 1a represents the observation equation, lines 1b through 1d specify the priors on the time varying mean,  $\beta_t$  and lines 1e through 1g specify the priors on the time varying log-variance,  $h_t$ . Application of BTF-ASV is explored in Section 6.

### 3 Parameter Estimation

In this section, we explore estimation of ASV model. Let's remind ourselves that ASV has the following hierarchical representation:

$$y_t = \exp\{h_t/2\}\epsilon_t \quad \epsilon_t \stackrel{iid}{\sim} N(0, 1) \quad (2a)$$

$$\Delta^k h_t = \omega_t = \exp\{v_t/2\}u_t \quad u_t \stackrel{iid}{\sim} N(0, 1) \quad (2b)$$

$$v_{t+1} = \mu + \phi(v_t - \mu) + \eta_t \quad \eta_t \stackrel{iid}{\sim} Z(a_\eta, b_\eta, 0, 1). \quad (2c)$$

$$\mu \sim Z(a_\mu, b_\mu, 0, 1) \quad (\phi + 1)/2 \sim Beta(a_\phi, b_\phi), \quad (2d)$$

where  $a_\eta, b_\eta, a_\mu, b_\mu, a_\phi$ , and  $b_\phi$  are hyperparameters. Define  $\mathbf{y} := (y_1, \dots, y_T)', \mathbf{h} := (h_1, \dots, h_T)',$  and  $\mathbf{v} := (v_1, \dots, v_T)'$ . The goal is to sample from the posterior distribution,  $f(\mathbf{h}, \mathbf{v}, \mu, \phi | \mathbf{y})$ . This may be achieved using Gibbs sampling, in which full conditional distribution for each variables,  $\mathbf{h}, \mathbf{v}, \mu$ , and  $\phi$  are sampled sequentially.

### 3.1 Parameter Expansion for the Likelihood

The difficulty in estimating the time-varying log-variance term  $h_t$  in SV model is its non-linear dependence in the likelihood. Sequential Monte Carlo by Jacquier et al. [1994] proposes sampling  $h_t$  sequentially, conditional on the past and future value of  $h_t$ . However, this method is indeed computationally intensive. Instead, we define  $y_t^* := \log(y_t^2)$ , and  $\mathbf{y}^* := (y_1^*, \dots, y_T^*)'$ , so that the model becomes linear system of equations with an unusual error term:

$$y_t^* = h_t + \log(\epsilon_t^2) \quad \epsilon_t \stackrel{iid}{\sim} N(0, 1).$$

We use the 10-component mixture Gaussian distribution by Omori et al. [2007] to approximate the non-Gaussian error term  $\epsilon_t^*$ :

$$y_t^* \approx h_t + \mu_{j_t} + \sigma_{j_t} o_t \quad o_t \stackrel{iid}{\sim} N(0, 1), \quad j_t \stackrel{iid}{\sim} \text{Categorical}(\pi)$$

The exact distribution for  $\pi$  can be found in Omori et al. [2007]. Conditional on the mixture component,  $j_t$ ,  $y_t^*$  is approximately a linear Gaussian State Space model where fast sampling of  $h_t$  becomes possible using the Cholesky factorization method proposed by Rue [2002]. Similarly, the change of variable and approximation is performed on  $\omega_{h,t}^* := \log(\omega_{h,t}^2) = \log((\Delta^k h_t)^2)$  when estimating the log-variance parameters for BTF-ASV model.

### 3.2 Parameter Expansion for the Z-distribution

Lines 2c and 2d of Model 3 can be viewed as SV model, with an exception that  $\eta_t \sim Z(a_\eta, b_\eta, 0, 1)$ , instead of  $N(0, 1)$ . Using the mean-variance scale mixture representation of the  $Z$ -distribution as explored in Barndorff-Nielsen et al. [1982]:

$$\eta | \xi \sim N(\xi^{-1}(a_\eta - b_\eta)/2, \xi^{-1})$$

$$\xi \sim PG(a_\eta + b_\eta, 0)$$

$\xi \sim PG(b_\xi, c_\xi)$  is an infinite convolution of gamma random variables:

$$\xi \stackrel{D}{=} (2\pi^2)^{-1} \sum_{k=1}^{\infty} g_k \{(k - \frac{1}{2})^2 - c_\xi^2/(4\pi^2)^{-1}\},$$

where,  $g_k \stackrel{iid}{\sim} \text{gamma}(b_\xi, 1)$  and  $\stackrel{D}{=}$  indicates equality of distribution. Efficient sampling from Pólya-Gamma random variable is done via truncating an infinite sum as proposed by Polson et al. [2013]. With the parameter expansion, we may use efficient AWOL sampler proposed by Kastner and Frühwirth-Schnatter [2014] for sampling  $\mathbf{v}$ ,  $\mu$  and  $\phi$ .

### 3.3 Gibbs Sampling with Parameter Expansion

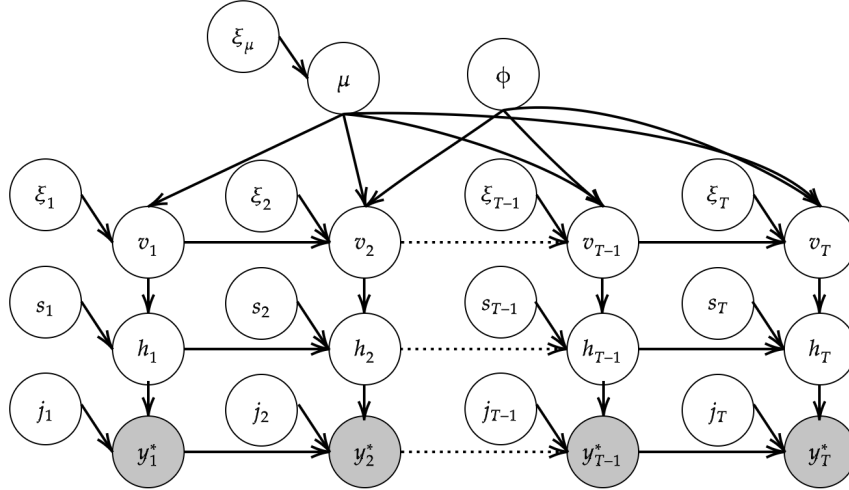


Figure 2: Graphical representations of Adaptive Stochastic Volatility with Dynamic Shrinkage Processes (ASV-DSP) with parameter expansions. In addition to the existing parameters,  $(\mathbf{h}, \mathbf{v}, \mu, \phi)$ , parameters  $(\mathbf{j}, \mathbf{s}, \boldsymbol{\xi}, \xi_\mu)$  are introduced for efficient Gibbs sampling.

Based on the approximations and parameter expansions explored in previous subsec-

tions, we have the following equation for ASV-DSP with  $a_\eta = b_\eta = a_\mu = b_\mu = 1/2$ :

$$\begin{aligned}
y_t^* &\approx h_t + \mu_{j_t} + \sigma_{j_t} o_t & o_t &\stackrel{iid}{\sim} N(0, 1) \\
\Delta^k h_t &= \omega_t^* \approx v_t + \mu_{s_t} + \sigma_{s_t} r_t & r_t &\stackrel{iid}{\sim} N(0, 1) \\
v_{t+1} &= \xi_\mu^{-1/2} \mu + \phi(v_t - \mu) + \xi_t^{-1/2} \eta_t & \eta_t &\stackrel{iid}{\sim} N(0, 1) \\
\mu &\sim N(0, 1) & \xi_\mu &\stackrel{iid}{\sim} PG(1, 0) \\
\xi_t &\stackrel{iid}{\sim} N(0, 1) & s_t &\stackrel{iid}{\sim} Categorical(\pi) \\
j_t &\stackrel{iid}{\sim} Categorical(\pi) & (\phi_h + 1)/2 &\sim Beta(a_\phi, b_\phi).
\end{aligned}$$

In addition to the four parameters in the original equation,  $\mathbf{h}$ ,  $\mathbf{v}$ ,  $\mu$ , and  $\phi$ , four additional parameters,  $\mathbf{j} := (j_1, \dots, j_T)'$ ,  $\mathbf{s} := (s_1, \dots, s_T)'$ ,  $\boldsymbol{\xi} := (\xi_1 \dots \xi_T)'$ , and  $\xi_\mu$  are introduced via parameter expansion and approximation.

Graphical representation ASV-DSP with parameter expansion is illustrated in Figure 2.

Define  $\theta^{1:T} = (\mathbf{j}, \mathbf{h}, \mathbf{v}, \mathbf{s}, \boldsymbol{\xi}, \mu, \xi_\mu, \phi)$  and  $\theta_{-j}^{1:T} = (\mathbf{h}, \mathbf{v}, \mathbf{s}, \boldsymbol{\xi}, \mu, \xi_\mu, \phi)$ . Similarly, define  $\theta_{-h}^{1:T}$  and so forth in a similar manner for all other variables. The following is the list of conditional distributions for Gibbs sampling. Despite the large number of parameters, many of the variables are conditionally independent, allowing efficient sampling scheme. The full conditional posterior distributions for Gibbs sampling are rigorously detailed in the supplementary material. Other than  $\phi$ , the closed form full conditional distribution was

used. Slice sampling by Neal [2003] were used for sampling  $\phi_h$ .

$$\begin{aligned}
f(\mathbf{j}|\theta_{-j}^{1:T}, \mathbf{y}^*) &= f(\mathbf{j}|\mathbf{h}, \mathbf{y}^*) \\
f(\mathbf{h}|\theta_{-h}^{1:T}, \mathbf{y}^*) &= f(\mathbf{h}|\mathbf{j}, \mathbf{v}, \mathbf{s}, \mathbf{y}^*) \\
f(\mathbf{v}|\theta_{-v}^{1:T}, \mathbf{y}^*) &= f(\mathbf{v}|\mathbf{s}, \mathbf{h}, \mu, \phi, \boldsymbol{\xi}) \\
f(\mathbf{s}|\theta_{-s}^{1:T}, \mathbf{y}^*) &= f(\mathbf{s}|\mathbf{h}, \mathbf{v}) \\
f(\boldsymbol{\xi}|\theta_{-\xi}^{1:T}, \mathbf{y}^*) &= f(\boldsymbol{\xi}|\mathbf{v}, \mu, \phi) \\
f(\mu|\theta_{-\mu}^{1:T}, \mathbf{y}^*) &= f(\mu|\mathbf{v}, \boldsymbol{\xi}, \xi_\mu, \phi) \\
f(\xi_\mu|\theta_{-\xi_\mu}^{1:T}, \mathbf{y}^*) &= f(\xi_\mu|\mu) \\
f(\phi|\theta_{-\phi}^{1:T}, \mathbf{y}^*) &= f(\phi|\mathbf{v}, \boldsymbol{\xi}, \mu)
\end{aligned}$$

For the posterior distribution  $f(\theta^{1:T} | \mathbf{y}^*)$ , each parameter is initialized appropriately and then sampled sequentially from the eight conditional distributions shown above until convergence. A similar Gibbs sampling approach is used for BTF-ASV.

## 4 Simulation Study

### 4.1 Set-up

So far, we have introduced three new volatility models: RWSV-BL, and two variants of ASV: ASV-DSP, and ASV-HS. The aim of the simulation study is to compare these models with established models, including SV, Markov-Switching SV with 2 Regimes (MSSV2), RWSV, GARCH, and Markov-Switching GARCH with 2 regimes (MSGARCH2). Assessing volatility models is challenging because true underlying volatility is unobservable in empirical data analysis. We evaluate model performance by testing their accuracy across wide array of data generating scenarios (DGSSs). We generate 10,000 sample paths with 1,000 data points each for six DGSSs outlined in Table 1. Note that SV, MSSV2, GARCH, and MSGARCH2 are the perfectly specified models for DGSSs 1, 2, 4, and 5 respectively

DGS1: SV with 1 Regime	DGS4: GARCH with 1 Regime
$h_{t+1} = 3 + 0.8(h_t - 3) + 0.2u_t$	$\sigma_{t+1}^2 = 1 + 0.1y_t^2 + 0.5\sigma_t^2$
DGS2: SV with 2 Regimes	DGS5: GARCH with 2 Regimes
$h_{t+1} = m_{s_{t+1}} + 0.8(h_t - m_{s_t}) + 0.2u_t$ $m_{s_t} = \begin{cases} -10, & \text{if } s_t = 0. \\ 6, & \text{if } s_t = 1. \end{cases}$	$\sigma_{t+1}^2 = m_{s_{t+1}} + 0.15y_t^2 + \beta_{s_{t+1}}\sigma_t^2$ $m_{s_t} = \begin{cases} 0.5, & \text{if } s_t = 0. \\ 0.1, & \text{if } s_t = 1. \end{cases}$ $\beta_{s_{t+1}} = \begin{cases} 0.8, & \text{if } s_t = 0. \\ 0.3, & \text{if } s_t = 1. \end{cases}$
DGS3: SV with 3 Regimes	DGS6: GARCH with 3 Regimes
$h_{t+1} = m_{s_{t+1}} + 0.8(h_t - m_{s_t}) + 0.2u_t$ $m_{s_t} = \begin{cases} -10, & \text{if } s_t = 0. \\ -3, & \text{if } s_t = 1. \\ 3, & \text{if } s_t = 2. \end{cases}$	$\sigma_{t+1}^2 = m_{s_{t+1}} + 0.15y_t^2 + \beta_{s_{t+1}}\sigma_t^2$ $m_{s_t} = \begin{cases} 2, & \text{if } s_t = 0. \\ 1, & \text{if } s_t = 1. \\ 0.01, & \text{if } s_t = 2. \end{cases}$ $\beta_{s_{t+1}} = \begin{cases} 0.8, & \text{if } s_t = 0. \\ 0.5, & \text{if } s_t = 1. \\ 0.2, & \text{if } s_t = 2. \end{cases}$

Table 1: Detailed summary of Data Generating Schemes (DGS) for the simulation study. Define  $y_t = \sigma_t \epsilon_t$ ,  $\epsilon_t \stackrel{iid}{\sim} N(0, 1)$ ,  $u_t \stackrel{iid}{\sim} N(0, 1)$ ,  $h_t := \log(\sigma_t^2)$ . Sample paths were generated from the stochastic volatility model with 1, 2, and 3 regimes for DGS 1, 2, and 3, respectively, and from the GARCH model with 1, 2, and 3 regimes for DGS 4, 5, and 6, respectively. Transitions between states 0 and 1 for DGS 2 and DGS 4 are governed by the following transition matrix  $\begin{pmatrix} 0.98 & 0.02 \\ 0.02 & 0.98 \end{pmatrix}$ . Transitions between states 0, 1 and 2 for DGS 3 and DGS 6 are governed by  $\begin{pmatrix} 0.98 & 0.01 & 0.01 \\ 0.01 & 0.98 & 0.01 \\ 0.01 & 0.01 & 0.98 \end{pmatrix}$ . Each DGS comprises 10,000 sample paths, each path being 1000 data points in length. Parameters for each DGS are detailed above.

and are expected to perform the best in their respective DGSs. In DGS 3 and 6, none of the models are correctly specified. These scenarios test each model's performance under misspecification. Prediction errors are measured using in-sample Mean Absolute Error (MAE) against log-variance  $h_t$  for DGS 1-3 and volatility  $\sigma_t$  for DGS 4-6:

$$MAE(\hat{h}) = \frac{1}{T} \sum_{t=1}^T |h_t - \hat{h}_t| \quad MAE(\hat{\sigma}) = \frac{1}{T} \sum_{t=1}^T |\sigma_t - \hat{\sigma}_t|.$$

Different sets of models are compared across two groups of data generating scenar-

ios: DGS 1 through 3 and DGS 4 through 6. In DGS 1 through 3, GARCH and MSGARCH2 models are not compared because the true volatility paths are represented by the log-variance process  $h_t$  rather than the volatility process  $\sigma_t$ , putting these models at a disadvantage. Similarly, SV, MSSV2, and RWSV are not compared in DGS 4 through 6 as these models are parameterized in terms of the log variance instead of the variance. ASV, our proposed models, however, are compared against other models in all 6 DGSs to demonstrate its local adaptivity.

SV, RWSV-BL, ASV-HS, and ASV-DSP all use Bayesian framework; MAE are calculated in terms of their posterior means on  $h_t$ . GARCH and MSGARCH model, on the other hand, are implemented in frequentist framework and the expected  $\sigma_t$  was used to compute  $MAE(\hat{\sigma})$ . For DGS 4 through 6, the posterior samples for  $h_t$  from the Bayesian models are first transformed to  $\sigma_t$ , and averaged to estimate the posterior mean of  $\sigma_t$ .

All models are implemented in R language (R Core Team [2013]). Specifically, SV model is implemented via stochvol (Kastner [2016]) package, MSSV2 as specified in Hamilton [1989] and RWSV are implemented by the authors as no readily available packages in R exists. GARCH(1,1) models are fitted via fGarch (Wuertz et al. [2023]) package, and MSSV2 are fitted via MSGARCH (Ardia et al. [2019]) package. For fitting RWSV-BL, dsp package by Kowal et al. [2019] and genlasso package by Arnold and Tibshirani [2022] are used. dsp package by Kowal et al. [2019] is further expanded to implement ASV models. For all Bayesian models, 5,000 posterior samples are generated after 20,000 burn-ins for each sample path.

## 4.2 Result

As shown in Figure 3, SV, MSSV2, GARCH, and MSGARCH2 exhibit the lowest average MAE across DGS 1,2,4, and 5, respectively as they represent the perfectly specified

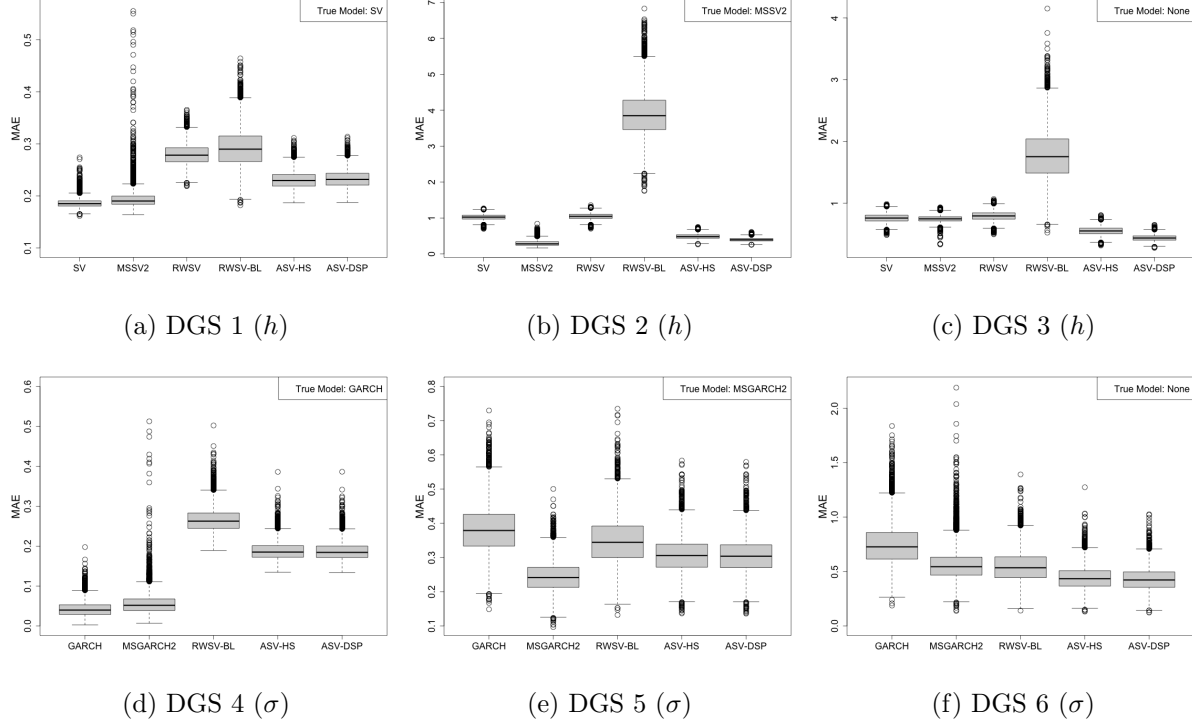


Figure 3: Box plots of Mean Absolute Error (MAE) across 10,000 sample paths measured in  $h$  for Data Generating Scenarios (DGS) 1, 2 and 3, and in  $\sigma$  for DGS 4, 5, and 6. Stochastic Volatility (SV), Markov-Switching Stochastic Volatility with 2 Regimes (MSSV2), Random Walk Stochastic Volatility with Inverse Gamma Prior (RWSV), Random Walk Stochastic Volatility with Bayesian LASSO (RWSV-BL), and Adaptive Stochastic Volatility with Dynamic Horseshoe Prior (ASV-HS), and ASV with Dynamic Shrinkage Processes (ASV-DSP) are compared in DGS 1, 2 and 3. Generalized AutoRegressive Conditional Heteroskedasticity (GARCH), Markov-Switching GARCH with 2 regimes (MSGARCH2), RWSV, RWSV-BL, ASV-HS, and ASV-DSP are compared in DGS 4, 5 and 6. For fair comparisons between models, the same 10,000 sample paths are used for all models to calculate the loss. Perfectly specified models are SV and MSSV2 for DGS 1 and 2 and GARCH and MSGARCH2 for DGS 4 and 5, respectively. All models are misspecified for DGS 3 and 6.

models. RWSV generally demonstrates similar or slightly worse accuracy compared to the SV model, while RWSV-BL performs notably poorly when compared to all other models, especially in DGS 1, 2, and 3. Despite its intended use in trend-filtering, Bayesian LASSO shows similar or lower accuracy in estimating time-varying volatility compared to the same model with a non-informative Inverse Gamma prior.

ASV, while not as accurate as the correctly specified models, demonstrate only a marginal difference in performance in DGS 1 and 2. ASV models are also close second

to MSSV2 in DGS 2, outperforming the SV model significantly. ASV models exhibit slightly poorer performance against GARCH and MSGARCH2 in DGS 4 due to the model misspecification, but is a close second to the correctly specified model in DGS 5, outperforming GARCH. In DGS 3 and 6, no models are correctly specified. In these scenarios, ASV models perform noticeably better than all other models, highlighting their ability to estimate arbitrary volatility processes. Across all DGSs, ASV ranks close to the correctly specified models and outperforms the established model in DGS 3 and 6. This is especially impressive considering ASV is misspecified in all six DGSs. The ASV-DSP and ASV-HS variants perform similarly across all six scenarios, with ASV-DSP being slightly more accurate in DGS 2 through 6. The performance difference is more pronounced in DGS 2 and 3. For detailed comparisons, additional box plots are provided in Appendix C.

Both of the compared Markov Switching type models, MSSV2 and MSGARCH2, appear to be less desirable than ASV models. As mentioned above, MSSV2 and MSGARCH2 both performed worse than the ASV models. Also in DGS 1 and 4, despite having lower median MAE, MSSV2 and MSGARCH2 both exhibit extremely large variances in their predictions. This may be because the models assume two regimes in the underlying volatility process. While they usually estimate the volatility process correctly, they sometimes assign a small probability to a non-existent second regime, resulting in a few widely inaccurate estimates.

Simulation study highlights ASV's ability to approximate true volatility paths across various DGSs with arbitrary number of abrupt changes in the volatility process. ASV models appear to perform especially well when there are multiple changes in the process as evident in DGS 2, 3, 5, and 6. The study also highlights apparent weakness of Markov Switching SV and GARCH models. While they are accurate when correctly specified, their performance significantly declines when misspecified. Thus, ASV models prove to

be a versatile framework capable of approximating arbitrary with varying regime changes without prior knowledge. In empirical data analysis, where the true data generating process is seldom known, ASVs holds a distinct advantage over existing models.

## 5 Empirical Study

### 5.1 Set-up

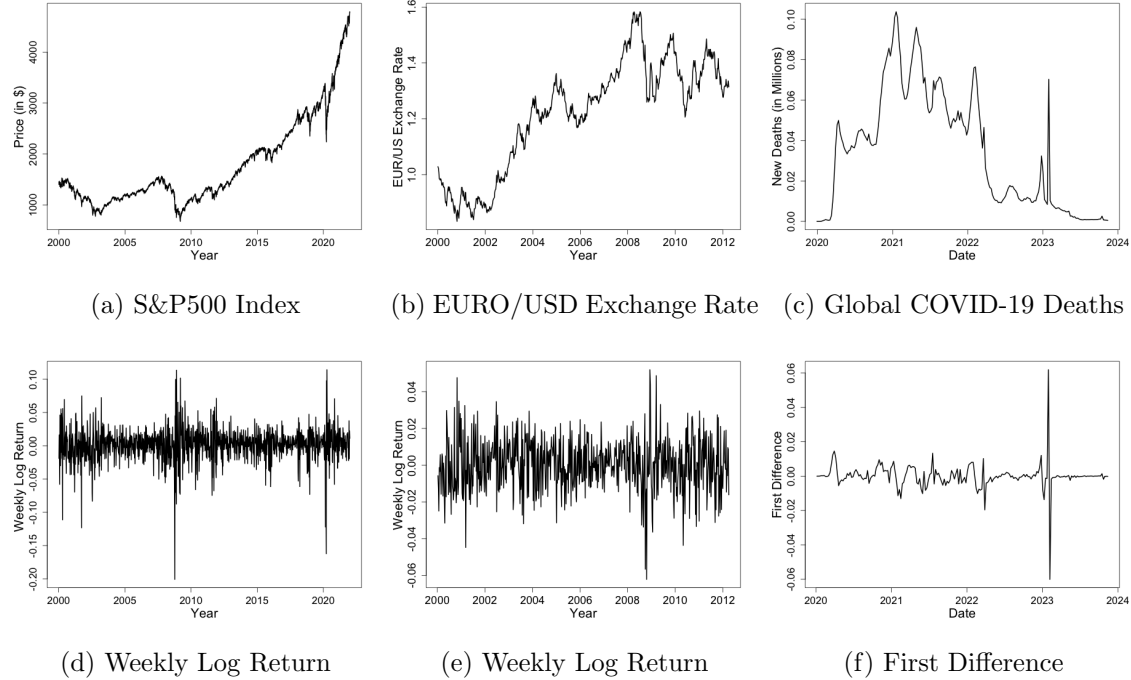


Figure 4: Price of S&P500 between 2012-01-01 and 2021-12-31 (a), EURO/USD exchange rate between 2000-01-03 and 2012-04-04 (b) and weekly COVID-19 new death tolls between 2020-01-03 to 2023-11-13 (c) in the United States are drawn. The weekly log return series for S&P500 and the exchange rate series are drawn in (d) and (e). The first difference series of COVID-19 death tolls are drawn in (f).

We apply ASV-DSP to empirical datasets and compare its volatility estimates with those from Stochastic Volatility (SV) and Random Walk Stochastic Volatility (RWSV) models. Specifically, we analyze the price of S&P500 from 2012-01-01 to 2021-12-31 ( $n = 1148$ , Figure 4a), EURO to US Dollar exchange rate between 2000-01-03 to 2012-04-04 ( $n = 639$ , Figure 4b), and new deaths from COVID-19 from 2020-01-03 to 2023-11-13 ( $n = 1148$ , Figure 4c).

202, Figure 4c). ASV model is applied to the weekly log return series for S&P 500 and EURO/USD exchange (Figure 4d and Figure 4e), and the weekly first difference series for COVID-19 death tolls in the U.S. (Figure 4f).

## 5.2 Results

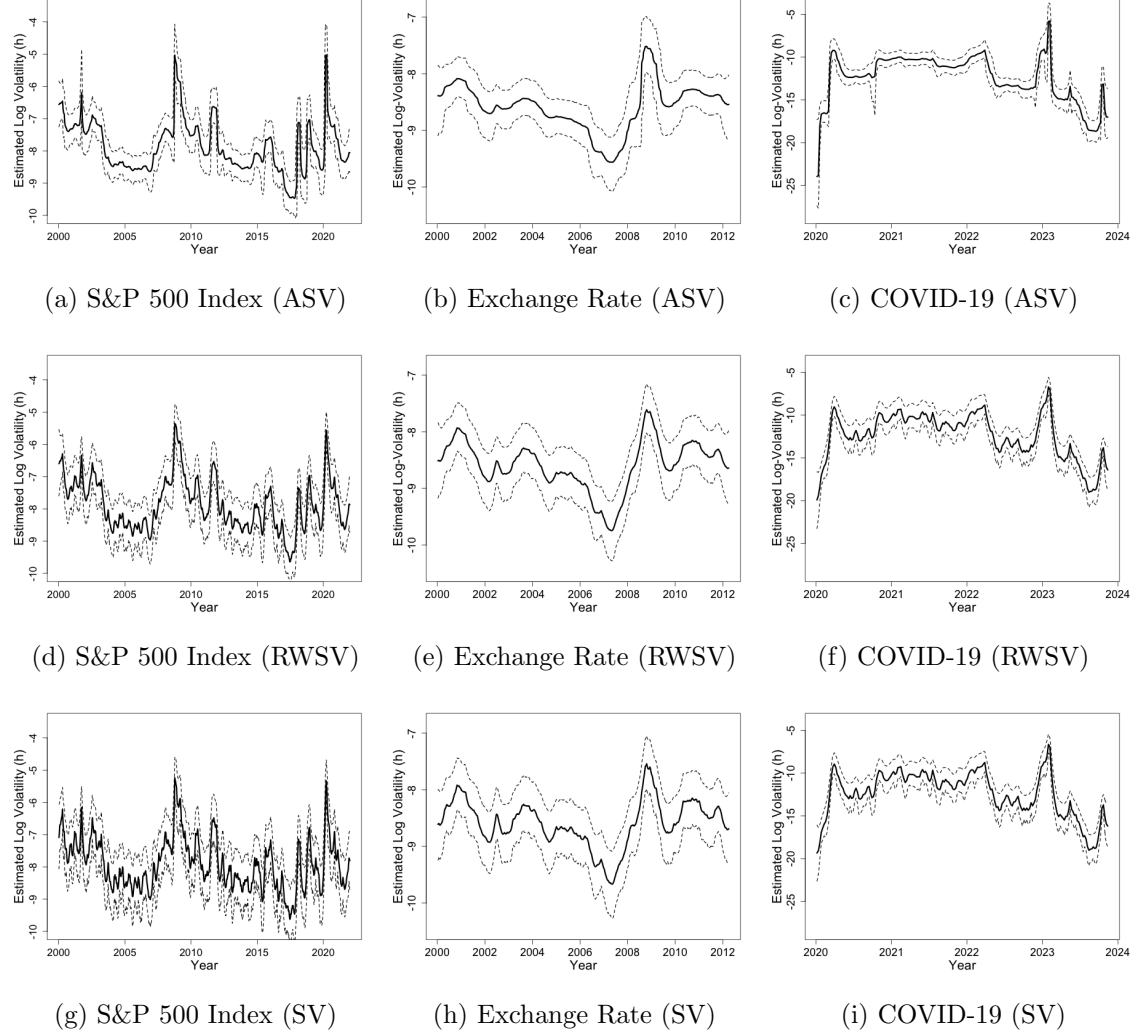


Figure 5: Estimated  $h$  with 90% quantile-based credible regions on weekly returns on S&P 500 between 2000-01-01 and 2021-12-31, weekly returns on EURO/USD exchange rate between 2000-01-03 and 2012-04-04, and weekly changes in COVID-19 death tolls in the U.S. between 2020-01-03 and 2023-11-13 based on Adaptive Shrinkage Process with Dynamic Shrinkage Process (ASV-DSP) shown in (a),(b), and (c), based on Random Walk Stochastic Volatility with inverse Gamma prior (RWSV) shown in (d), (e), and (f) and based on Stochastic Volatility (SV) model shown in (g),(h), and (i).

We first assess the log-volatility ( $h_t$ ) estimates generated by ASV-DSP in comparison

with RWSV and SV model across three data sets (Figure 5). Focusing on the S&P 500 dataset (Figures 5a, 5d and 5g), the most prominent features are the two large spikes in 2009 and 2020 due to financial crisis and COVID-19 outbreaks. In terms of moderate changes, the one around 2001 coincides with 9/11 attack and the 2011 surge aligns with the European Debt crisis, both of which caused a stock market decline. The stock market in 2018 followed the strongest 2017 market since the financial crisis but was overall exhibited extreme volatility, likely due to U.S. government shut down early and late in that year. While discernible in ASV, small to moderate changes in volatility is hard to distinguish from noise in noisier estimates from SV and RWSV.

The EURO/USD exchange rate's most notable volatility pattern includes a steady decline from 2001 to 2008, a substantial spike in 2008 and 2009 due to the financial crisis, and a minor bump in 2010 and 2011, likely tied to the European Debt crisis as well (Figures 5b, 5e and 5h). Figure 4b suggests a steady increase in the EURO/USD exchange rate between 2001 and 2008, resulting in low volatility. ASV, RWSV and SV all exhibit a very similar pattern, with ASV displaying a smoother output than those of RWSV and SV. Because of this, The steady decline in volatility from 2001 to 2007 is easier to notice from ASV than from both SV and RWSV.

A discernible pattern from all three models for COVID-19 death tolls is the significant volatility spike occurring around the onset of the pandemic in early 2020 and another one in early 2023 (Figures 5c, 5f and 5i). Subsequently, seasonal effect appears to be present; there are small to large increases in volatility at the end and beginning of each year, followed by reductions in the summer months, particularly noticeable in 2022 and 2023. In mid-2022, a substantial dip in volatility is observed, succeeded by a notable spike toward the end of 2022 and the beginning of 2023. By the mid-2023, volatility plateaus, and experience dramatic

decline, only to exhibit another spike by the end of 2023. This pattern is also observed to a lesser extent in 2020 and 2021, according to estimates from ASV. Such pattern is less noticeable based on estimates from both SV and RWSV.

All three models' estimates appear to share the same overall pattern, but with varying degree of smoothness. ASV generates the smoothest estimate out of the three models followed by RWSV and SV across the three data sets. A key advantage of this enhanced smoothness is improved interpretability. As discussed earlier, ASV-DSP excels, particularly in discerning small to medium changes in volatility, offering better clarity in distinguishing signal from noise compared to SV or RWSV, whose outputs tend to be noisier, rendering signals often indistinguishable from the noise. The reduced noise in ASV's output enables users to gain a clearer understanding of underlying patterns and trends.

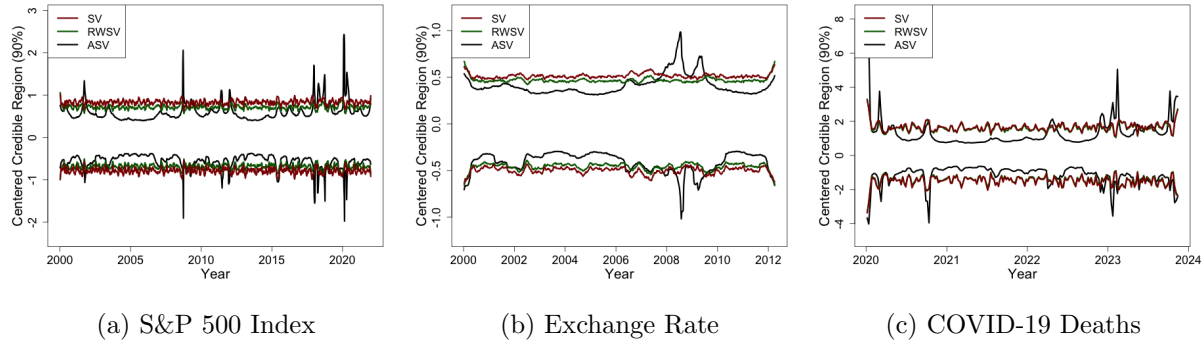


Figure 6: The 90% quantile-based credible regions on the log-variance  $h_t$  are subtracted by its posterior sample mean. The three datasets include weekly returns on S&P 500 between 2000-01-01 and 2021-12-31, weekly returns on EURO/USD exchange rate between 2000-01-03 and 2012-04-04, and weekly changes in COVID-19 death tolls between 2020-01-03 and 2023-11-13 in the U.S. The centered credible regions for Adaptive Stochastic Volatility with Dynamic Shrinkage Processes (ASV-DSP) are drawn in black, the ones based on Stochastic Volatility (SV) model are in dark red and the ones based on Random Walk Stochastic Volatility (RWSV) model are in dark green.

Another distinguishing feature of ASV is its locally adaptive credible region. Due to time-varying variance term  $\tau \lambda_t = \exp\{v_t/2\}$ , credible region around  $h_t$  produced by ASV-DSP also changes over time. The mean-centered credible regions generated by SV, RWSV

and ASV on the three data sets are illustrated in Figure 6. Notably, the credible regions maintain a constant width for both SV and RWSV model across the sample path with RWSV having slightly narrower credible region. The credible region around  $h$  for ASV, on the other hand, exhibits local adaptability. Specifically, the patterns on the centered credible regions match that of  $h_t$  explored in previous paragraphs. When changes in  $h_t$  are slow moving, the width of the credible region is narrow; while abrupt changes in  $h_t$  induce large credible regions.

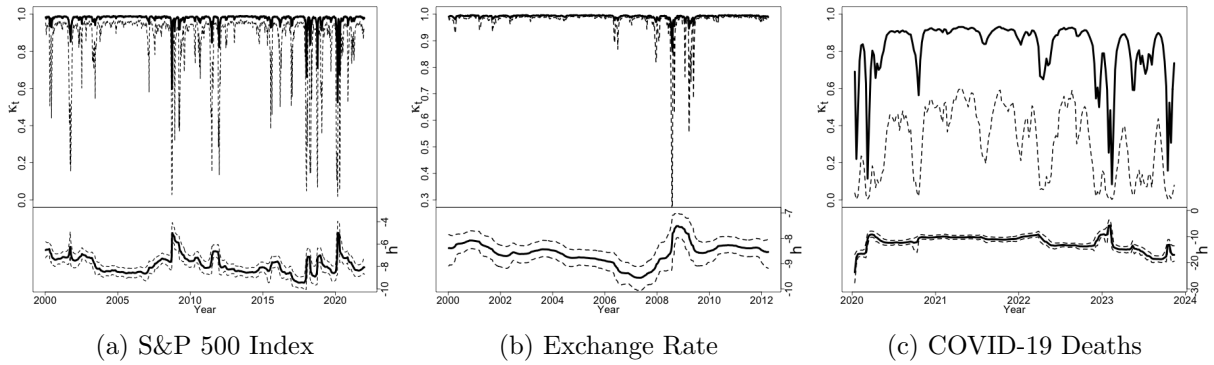


Figure 7: Comparison between the expected shrinkage parameter  $\kappa_t := \frac{1}{1+\text{var}(\omega_t|\tau, \lambda_t)} = \frac{1}{1+\exp\{v_t\}} = \frac{1}{1+\tau^2\lambda_t^2}$  and expected  $h_t$  based on Adaptive Stochastic Volatility with Dynamic Shrinkage Processes (ASV-DSP) estimated on weekly returns on S&P 500 between 2000-01-01 and 2021-12-31, weekly returns on EURO/USD exchange rate between 2000-01-03 and 2012-04-04, and weekly changes in COVID-19 death tolls in the U.S. between 2020-01-03 and 2023-11-13, respectively. The dotted lines represent the one-sided 95th and centered 90th percentile credible regions for  $\kappa_t$  and  $h_t$  respectively.

Lastly, we analyze the empirical shrinkage parameter  $\kappa_t$ . The parameter  $v_t$  represents the log-variance term of  $\Delta h_t$ . A small  $v_t$  corresponds to minor changes in  $h_t$ , while a large  $v_t$  signifies substantial variations. Alternatively,  $v_t$  can be seen as influencing the degree of shrinkage applied to  $h_t$ , denoted as  $\kappa_t := \frac{1}{1+\text{var}(\omega_t|\tau, \lambda_t)} = \frac{1}{1+\exp(v_t)} = \frac{1}{1+\tau^2\lambda_t^2}$ . Analyzing  $\kappa_t$  rather than  $v_t$  is preferred for clarity since  $\kappa_t \in (0, 1)$ , unlike  $v_t \in (-\infty, +\infty)$ . A high  $\kappa_t$  (near 1) indicates strong model certainty, while a low  $\kappa_t$  (near 0) indicates less certainty in the estimate. Figure 7 shows the comparison between the estimated log-volatility  $h_t$  and the shrinkage parameter  $\kappa_t$ . As expected in ASV, prominent peaks in  $h_t$  correspond

to  $\kappa_t$  values near 0. During periods of gradual evolution,  $\kappa_t$  is close to 1. Generally,  $\kappa_t$  for the COVID-19 deaths data is more volatile than for the S&P 500 and exchange rate data, indicating lower certainty in the model's estimates. This could be due to the smaller sample size of the COVID-19 dataset (203 data points) compared to the S&P 500 (1148 data points) and exchange rate (639 data points) datasets.

## 6 Trend Filtering Jointly in Mean and Variance

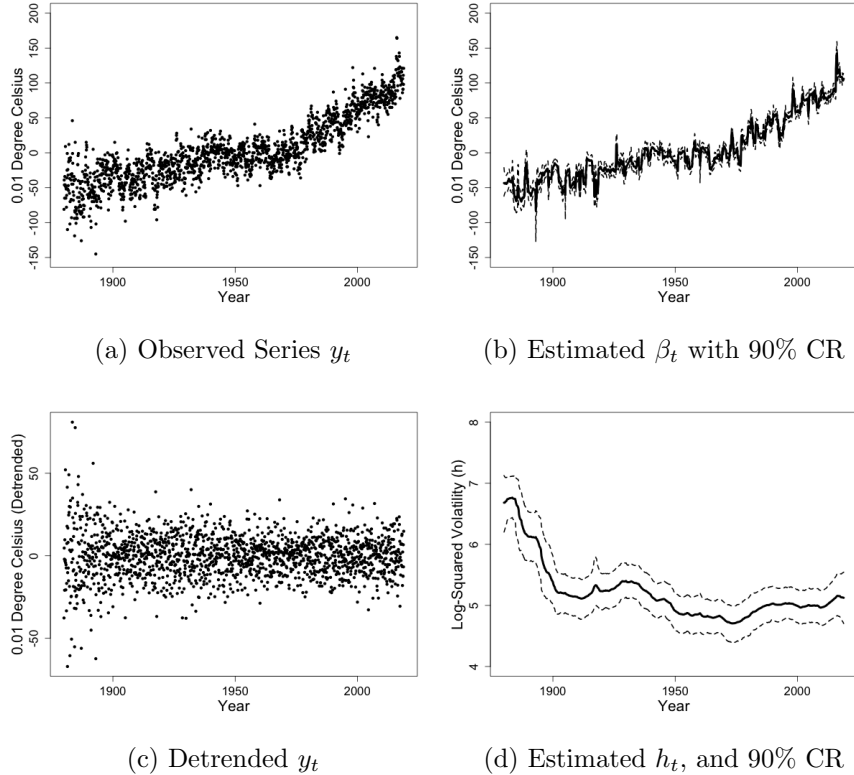


Figure 8: The monthly average global land surface air temperature anomaly from 1880 to 2018 with average temperature between 1950 and 1980 as base is illustrated in figure (a). Bayesian Trend Filter with Adaptive Stochastic Volatility is used to estimate the mean trend  $\beta_t$  and is illustrated in (b) with 90% credible region. Posterior mean for  $\beta_t$  was subtracted from the observed series to detrend the series and are illustrated in (c). BTF-ASV estimate of log-variance,  $h_t$  and its 90% credible regions is shown in (d).

Kowal et al. [2019] applies the DSP to Dynamic Linear Model and refers to the model as Bayesian Trend Filter with Dynamic Shrinkage Processes (BTF-DSP). We extend BTF-DSP by incorporating ASV on its error process. The resulting model provide smooth yet

locally adaptive estimate of both the mean process  $\beta_t$  and the log variance process  $h_t$ . Exact specification of the model is discussed in Model 1. In this section, we apply this method to analyze monthly global land surface air temperature anomaly with reference period 1951-1980 in 0.01 degree Celsius from 1880 to 2018. The data maybe found in this url: [https://data.giss.nasa.gov/gistemp/tabledata\\_v3/GLB.Ts.txt](https://data.giss.nasa.gov/gistemp/tabledata_v3/GLB.Ts.txt).

The global temperature has demonstrated a consistent upward trend from 1880 to 2018 (Figure 6). This is reflected in the estimated posterior mean for  $\beta$ , showing a similar but smoother pattern. It is important to note that despite the model's tendency to generate a smooth estimate, local trends still persist. This is likely attributed to yearly seasonal fluctuations as well large scale climate pattern such as El Niño and La Niña. Furthermore, there is a discernible shift in volatility over time. Notably, before 1900, extreme temperatures occurred more frequently, with wider range of fluctuations in temperature. Post-1900, however, temperatures remained within a narrower range, with occasional outliers. This pattern is captured by our estimation of log variance. The calculated volatility peaks around 1880 and gradually decreases until 1900. Subsequently, between 1900 and 2018, volatility appears to stabilize, as illustrated in Figure 6.

## 7 Conclusion

In this paper, we extend the RWSV model to create a flexible and adaptive framework for modeling time-varying volatility with both abrupt and gradual changes. Initially, we introduce RWSV-BL, incorporating the time-varying variance of  $\Delta h_t$  with a popular shrinkage prior, Bayesian LASSO. However, our simulation study reveals that RWSV-BL is suboptimal compared to RWSV with a non-informative prior. To address this, we enhance RWSV-BL by applying a global-local shrinkage prior to the variance of  $\Delta h_t$ , leading to the development of ASV.

We utilize a specific global-local shrinkage prior known as DSP introduced by Kowal et al. [2019] to develop two versions of ASV: ASV-HS and ASV-DSP. Extensive simulation studies show that both ASV-HS and ASV-DSP consistently outperform or match established models in terms of their accuracy. Especially, ASV exhibits resilience against model misspecification biases, underscoring its robustness, particularly in scenarios where the true data-generating process is unknown. Empirical studies demonstrate that ASV distinguishes itself from other models by generating smooth yet locally adaptive outputs, providing more interpretable results for users. ASV emerges as a powerful tool for estimating arbitrary volatility processes.

Finally, we integrate ASV into the error process of the Bayesian Trend Filter proposed in Kowal et al. [2019], resulting in BTF-ASV. Empirical studies reveal that this model is capable of producing smooth estimates of both time-varying mean and time-varying variance. Future research directions could explore the applications of ASV and DSP-ASV in diverse fields such as Finance, Environmental Science, and Epidemiology, leveraging their adaptability and robustness in modeling time-series exhibiting complex patterns.

## 8 Acknowledgement

Financial support from National Science Foundation grants OAC-1940124 and DMS-2114143 is gratefully acknowledged.

## 9 Supplementary Material

**Appendices:** A document including detailed proofs on the properties of Dynamic Shrinkage Processes (DSP) in section A, the exact prior distributions and detailed derivations of the full conditional distributions for Gibbs sampling in section B, and an additional figure shown in Figure 3, but excluding the results from the Random Walk Stochastic Volatility model with Bayesian LASSO.

## References

Jorge Achcar, Ricardo de Oliveira, and Emerson Barili. Use of stochastic volatility models in epidemiological data: Application to a dengue time series in São Paulo city, Brazil. *Journal of Biostatistics and Epidemiology*, 6(1):19–29, Oct. 2020. doi: 10.18502/jbe.v6i1.4755. URL <https://jbe.tums.ac.ir/index.php/jbe/article/view/338>.

David Ardia, Keven Bluteau, Kris Boudt, and Leopoldo Catania. Forecasting risk with markov-switching garch models: A large-scale performance study. *International Journal of Forecasting*, 34(4):733–747, 2018.

David Ardia, Keven Bluteau, Kris Boudt, Leopoldo Catania, and Denis-Alexandre Trotter. Markov-switching garch models in r: The msgarch package. *Journal of Statistical Software*, 91(4):1–38, 2019. doi: 10.18637/jss.v091.i04.

Taylor B. Arnold and Ryan J. Tibshirani. *genlasso: Path Algorithm for Generalized Lasso Problems*, 2022. URL <https://CRAN.R-project.org/package=genlasso>. R package version 1.6.1.

O. Barndorff-Nielsen, J. Kent, and M. Sørensen. Normal variance-mean mixtures and z distributions. *International Statistical Review / Revue Internationale de Statistique*, 50(2):145–159, 1982. ISSN 03067734, 17515823. URL <http://www.jstor.org/stable/1402598>.

Luc Bauwens, Arie Preminger, and Jeroen V. K. Rombouts. Theory and inference for a markov switching garch model. *The Econometrics Journal*, 13(2):218–244, 2010. ISSN 13684221, 1368423X. URL <http://www.jstor.org/stable/23117467>.

Anindya Bhadra, Jyotishka Datta, Nicholas G. Polson, and Brandon Willard. The horseshoe+ estimator of ultra-sparse signals, 2015.

Tim Bollerslev. Generalized autoregressive conditional heteroskedasticity. *Journal of Econometrics*, 31(3):307–327, 1986. ISSN 0304-4076. doi: [https://doi.org/10.1016/0304-4076\(86\)90063-1](https://doi.org/10.1016/0304-4076(86)90063-1). URL <https://www.sciencedirect.com/science/article/pii/0304407686900631>.

Celso Brunetti, Chiara Scotti, Roberto S Mariano, and Augustine HH Tan. Markov switching garch models of currency turmoil in southeast asia. *Emerging Markets Review*, 9(2):104–128, 2008.

Annalisa Cadonna, Sylvia Frühwirth-Schnatter, and Peter Knaus. Triple the gamma – a unifying shrinkage prior for variance and variable selection in sparse state space and tvp models, 2019.

Jun Cai. A markov model of switching-regime arch. *Journal of Business & Economic Statistics*, 12(3):309–316, 1994. ISSN 07350015. URL <http://www.jstor.org/stable/1392087>.

Guglielmo Maria Caporale and Timur Zekokh. Modelling volatility of cryptocurrencies using markov-switching garch models. *Research in International Business and Finance*, 48:143–155, 2019.

CARLOS M. Carvalho, NICHOLAS G. POLSON, and JAMES G. SCOTT. The horseshoe estimator for sparse signals. *Biometrika*, 97(2):465–480, 2010. ISSN 00063444, 14643510. URL <http://www.jstor.org/stable/25734098>.

Ray Yeutien Chou. Volatility persistence and stock valuations: Some empirical evidence using garch. *Journal of Applied Econometrics*, 3(4):279–294, 1988. ISSN 08837252, 10991255. URL <http://www.jstor.org/stable/2096644>.

Michael J Dueker. Markov switching in garch processes and mean-reverting stock-market volatility. *Journal of Business & Economic Statistics*, 15(1):26–34, 1997.

Robert F. Engle. Autoregressive conditional heteroscedasticity with estimates of the variance of united kingdom inflation. *Econometrica*, 50(4):987–1007, 1982. ISSN 00129682, 14680262. URL <http://www.jstor.org/stable/1912773>.

Kenneth French, G. Schwert, and Robert Stambaugh. Expected stock returns and volatility. *Journal of Financial Economics*, 19(1):3–29, 1987. URL <https://EconPapers.repec.org/RePEc:eee:jfinec:v:19:y:1987:i:1:p:3-29>.

Stephen F. Gray. Modeling the conditional distribution of interest rates as a regime-switching process. *Journal of Financial Economics*, 42(1):27–62, September 1996. URL <https://ideas.repec.org/a/eee/jfinec/v42y1996i1p27-62.html>.

James D. Hamilton. A new approach to the economic analysis of nonstationary time series and the business cycle. *Econometrica*, 57(2):357–384, 1989. ISSN 00129682, 14680262. URL <http://www.jstor.org/stable/1912559>.

James D Hamilton and Raul Susmel. Autoregressive conditional heteroskedasticity and changes in regime. *Journal of Econometrics*, 64(1):307–333, 1994. ISSN 0304-4076. doi: [https://doi.org/10.1016/0304-4076\(94\)90067-1](https://doi.org/10.1016/0304-4076(94)90067-1). URL <https://www.sciencedirect.com/science/article/pii/0304407694900671>.

Andrew Harvey, Esther Ruiz, and Neil Shephard. Multivariate stochastic variance models. *The Review of Economic Studies*, 61(2):247–264, 04 1994. ISSN 0034-6527. doi: 10.2307/2297980. URL <https://doi.org/10.2307/2297980>.

Florian Huber and Michael Pfarrhofer. Dynamic shrinkage in time-varying parameter stochastic volatility in mean models. *Journal of Applied Econometrics*, 36(2):262–270, 2021. doi: <https://doi.org/10.1002/jae.2804>. URL <https://onlinelibrary.wiley.com/doi/abs/10.1002/jae.2804>.

JOHN Hull and ALAN White. The pricing of options on assets with stochastic volatilities. *The Journal of Finance*, 42(2):281–300, 1987. doi: <https://doi.org/10.1111/j.1540-6261.1987.tb02568.x>. URL <https://onlinelibrary.wiley.com/doi/abs/10.1111/j.1540-6261.1987.tb02568.x>.

Soosung Hwang, Steve E. Satchell, and Pedro L. Valls Pereira. How Persistent is Volatility? An Answer with Stochastic Volatility Models with Markov Regime Switching State Equations. Econometric Society 2004 Latin American Meetings 198, Econometric Society, August 2004. URL <https://ideas.repec.org/p/ecm/latm04/198.html>.

Eric Jacquier, Nicholas G. Polson, and Peter E. Rossi. Bayesian analysis of stochastic volatility models. *Journal of Business & Economic Statistics*, 12(4):371–389, 1994. ISSN 07350015. URL <http://www.jstor.org/stable/1392199>.

Gregor Kastner. Dealing with stochastic volatility in time series using the R package stochvol. *Journal of Statistical Software*, 69(5):1–30, 2016. doi: 10.18637/jss.v069.i05.

Gregor Kastner and Sylvia Frühwirth-Schnatter. Ancillarity-sufficiency interweaving strategy (ASIS) for boosting MCMC estimation of stochastic volatility models. *Computational Statistics & Data Analysis*, 76:408–423, aug 2014. doi: 10.1016/j.csda.2013.01.002. URL <https://doi.org/10.1016%2Fj.csda.2013.01.002>.

Seung-Jean Kim, Kwangmoo Koh, Stephen Boyd, and Dimitry Gorinevsky.  $l_1$  trend filtering. *SIAM Rev.*, 51(2):339–360, 2009. ISSN 0036-1445,1095-7200. doi: 10.1137/070690274. URL <https://doi.org/10.1137/070690274>.

Polychronis Kostoulas, Eletherios Meletis, Konstantinos Pateras, Paolo Eusebi, Theodoros Kostoulas, Luis Furuya-Kanamori, Niko Speybroeck, Matthew Denwood, Suhail Doi, Christian Althaus, Carsten Kirkeby, Pejman Rohani, Navneet Dhand, José Peñalvo, Lehana Thabane, Ben miled Slimane, Hamid Sharifi, and Stephen Walter. The epidemic volatility index, a novel early warning tool for identifying new waves in an epidemic. *Scientific Reports*, 11:23775, 12 2021. doi: 10.1038/s41598-021-02622-3.

Daniel R. Kowal, David S. Matteson, and David Ruppert. Dynamic Shrinkage Processes. *Journal of the Royal Statistical Society Series B: Statistical Methodology*, 81(4):781–804, 05 2019. ISSN 1369-7412. doi: 10.1111/rssb.12325. URL <https://doi.org/10.1111/rssb.12325>.

Jiaxin Ma, Feiyun Xu, Kai Huang, and Ren Huang. Gnar-garch model and its application in feature extraction for rolling bearing fault diagnosis. *Mechanical Systems and Signal Processing*, 93:175–203, 2017.

Saeid Mehdizadeh, Javad Behmanesh, and Keivan Khalili. A comparison of monthly precipitation point estimates at 6 locations in iran using integration of soft computing methods and garch time series model. *Journal of Hydrology*, 554:721–742, 2017. ISSN 0022-1694. doi: <https://doi.org/10.1016/j.jhydrol.2017.09.056>. URL <https://www.sciencedirect.com/science/article/pii/S0022169417306601>.

Angelo Melino and Stuart M. Turnbull. Pricing foreign currency options with stochastic volatility. *Journal of Econometrics*, 45(1-2):239–265, 1990. URL <https://EconPapers.repec.org/RePEc:eee:econom:v:45:y:1990:i:1-2:p:239-265>.

Reza Modarres and Taha BMJ Ouarda. Modeling the relationship between climate oscillations and drought by a multivariate garch model. *Water Resources Research*, 50(1):601–618, 2014.

Radford M. Neal. Slice sampling. *The Annals of Statistics*, 31(3):705 – 767, 2003. doi: 10.1214/aos/1056562461. URL <https://doi.org/10.1214/aos/1056562461>.

Haruhisa Nishino and Kazuhiko Kakamu. A random walk stochastic volatility model for income inequality. *Japan and the World Economy*, 36:21–28, 2015. ISSN 0922-1425. doi: <https://doi.org/10.1016/j.japwor.2015.06.003>. URL <https://www.sciencedirect.com/science/article/pii/S0922142515000328>.

Yasuhiro Omori, Siddhartha Chib, Neil Shephard, and Jouchi Nakajima. Stochastic volatility with leverage: Fast and efficient likelihood inference. *Journal of Econometrics*, 140(2):425–449, 2007. ISSN 0304-4076. doi: <https://doi.org/10.1016/j.jeconom.2006.07.008>. URL <https://www.sciencedirect.com/science/article/pii/S0304407606001436>.

Martins Otache. Conditional heteroscedasticity in streamflow process: Paradox or reality? *Open Journal of Modern Hydrology*, 02:79–90, 01 2012. doi: 10.4236/ojmh.2012.24010.

Trevor Park and George Casella. The bayesian lasso. *Journal of the American Statistical Association*, 103(482):681–686, 2008. doi: 10.1198/016214508000000337. URL <https://doi.org/10.1198/016214508000000337>.

Hong Thom Pham and Bo-Suk Yang. Estimation and forecasting of machine health condition using arma/garch model. *Mechanical systems and signal processing*, 24(2):546–558, 2010.

Nicholas G. Polson, James G. Scott, and Jesse Windle. Bayesian inference for logistic models using polya-gamma latent variables, 2013.

Ser-Huang Poon and Stephen J. Taylor. Stock returns and volatility: An empirical study of the uk stock market. *Journal of Banking & Finance*, 16(1):37–59, 1992. ISSN 0378-4266. doi: [https://doi.org/10.1016/0378-4266\(92\)90077-D](https://doi.org/10.1016/0378-4266(92)90077-D). URL <https://www.sciencedirect.com/science/article/pii/037842669290077D>. Special Issue on European Capital Markets.

R Core Team. *R: A Language and Environment for Statistical Computing*. R Foundation for Statistical Computing, Vienna, Austria, 2013. URL <http://www.R-project.org/>.

Håvard Rue. Fast Sampling of Gaussian Markov Random Fields. *Journal of the Royal Statistical Society Series B: Statistical Methodology*, 63(2):325–338, 01 2002. ISSN 1369-7412. doi: 10.1111/1467-9868.00288. URL <https://doi.org/10.1111/1467-9868.00288>.

Esther Ruiz. Quasi-maximum likelihood estimation of stochastic volatility models. *Journal of Econometrics*, 63(1):289–306, 1994. ISSN 0304-4076. doi: [https://doi.org/10.1016/0304-4076\(93\)01569-8](https://doi.org/10.1016/0304-4076(93)01569-8). URL <https://www.sciencedirect.com/science/article/pii/0304407693015698>.

Rasoul Sajjad, Jerry Coakley, and John C Nankervis. Markov-switching garch modelling of value-at-risk. *Studies in Nonlinear Dynamics & Econometrics*, 12(3), 2008.

RR Sarkar and C Chatterjee. Application of different time series models on epidemiological data-comparison and predictions for malaria prevalence. *SM J. Biom. Biostat*, 2(4):1022, 2017.

Toryn L. J. Schafer and David S. Matteson. Locally adaptive shrinkage priors for trends and breaks in count time series. *to appear in Technometrics*. URL <https://arxiv.org/abs/2309.00080>.

Mike K. P. So, K. Lam, and W. K. Li. A stochastic volatility model with markov switching. *Journal of Business & Economic Statistics*, 16(2):244–253, 1998. ISSN 07350015. URL <http://www.jstor.org/stable/1392580>.

Mike K.P. So, K. Lam, and W.K. Li. An Empirical Study of Volatility in Seven Southeast Asian Stock Markets Using ARV Models. *Journal of Business Finance & Accounting*, 24 (2):261–276, March 1997. doi: 10.1111/1468-5957.00104. URL <https://ideas.repec.org/a/bla/jbfac/v24y1997i2p261-276.html>.

Fei Su and Lei Wang. Conditional volatility persistence and realized volatility asymmetry: Evidence from the chinese stock markets. *Emerging Markets Finance and Trade*, 56(14):3252–3269, 2020. doi: 10.1080/1540496X.2019.1574566. URL <https://doi.org/10.1080/1540496X.2019.1574566>.

S.J. Taylor. *Modelling Financial Time Series*. G - Reference,Information and Interdisciplinary Subjects Series. World Scientific, 2008. ISBN 9789812770844. URL <https://books.google.com/books?id=KQ5pDQAAQBAJ>.

Robert Tibshirani. Regression shrinkage and selection via the lasso. *Journal of the Royal Statistical Society. Series B (Methodological)*, 58(1):267–288, 1996. ISSN 00359246. URL <http://www.jstor.org/stable/2346178>.

Ryan J. Tibshirani. Adaptive piecewise polynomial estimation via trend filtering. *The Annals of Statistics*, 42(1), February 2014. ISSN 0090-5364. doi: 10.1214/13-aos1189. URL <http://dx.doi.org/10.1214/13-AOS1189>.

Michael K Tippett. Changing volatility of us annual tornado reports. *Geophysical Research Letters*, 41(19):6956–6961, 2014.

Huimin Wang, Songbai Song, Gengxi Zhang, Olusola O. Ayantobo, and Tianli Guo. Stochastic volatility modeling of daily streamflow time series. *Water Resources Research*, 59(1):e2021WR031662, 2023a. doi: <https://doi.org/10.1029/2021WR031662>. URL <https://agupubs.onlinelibrary.wiley.com/doi/abs/10.1029/2021WR031662>. e2021WR031662 2021WR031662.

Huimin Wang, Songbai Song, Gengxi Zhang, and Olusola O. Ayantoboc. Predicting daily streamflow with a novel multi-regime switching arima-ms-garch model. *Journal of Hydrology: Regional Studies*, 47:101374, 2023b. ISSN 2214-5818. doi: <https://doi.org/10.1016/j.ejrh.2023.101374>. URL <https://www.sciencedirect.com/science/article/pii/S2214581823000617>.

W Wang, PHAJ M Van Gelder, JK Vrijling, and J Ma. Testing and modelling autoregressive conditional heteroskedasticity of streamflow processes. *Nonlinear processes in Geophysics*, 12(1):55–66, 2005.

MIKE West. On scale mixtures of normal distributions. *Biometrika*, 74(3):646–648, 09 1987. ISSN 0006-3444. doi: 10.1093/biomet/74.3.646. URL <https://doi.org/10.1093/biomet/74.3.646>.

Haoxuan Wu, Toryn L. J. Schafer, and David S. Matteson. Trend and variance adaptive bayesian changepoint analysis and local outlier scoring. *Journal of Business & Economic Statistics*, 0(0):1–12, 2024a. doi: 10.1080/07350015.2024.2362269. URL <https://doi.org/10.1080/07350015.2024.2362269>.

Haoxuan Wu, Toryn L. J. Schafer, Sean Ryan, and David S. Matteson. Drift vs shift: Decoupling trends and changepoint analysis. *Technometrics*, 0(ja):1–16, 2024b. doi: 10.1080/00401706.2024.2365730. URL <https://doi.org/10.1080/00401706.2024.2365730>.

Diethelm Wuertz, Yohan Chalabi, Tobias Setz, Martin Maechler, and Georgi N. Boshnakov. *fGarch: Rmetrics - Autoregressive Conditional Heteroskedastic Modelling*, 2023. URL <https://www.rmetrics.org>. R package version 4031.90.

# A Proofs of Theorems

## A.1 Theorem 1

As mentioned, proofs directly follow from Kolmogorov's three series theorem, which state the sufficient and necessary condition for almost sure convergence of infinite sum of random variables. Let  $\phi \in (0, 1)$ . Due to symmetry of  $\text{sech}$  function, we only need to prove the case when  $0 < \phi < 1$ , and the case where  $-1 < \phi < 0$ , directly follows. For the first condition, let  $\epsilon > 0$ , and  $h$  is some positive integer or 0.

$$\begin{aligned}
P(|z_h| \geq \epsilon) &= 2 \int_{\epsilon}^{\infty} \frac{\exp\{x/(2\phi^h)\}}{\pi\phi^h(1 + \exp\{x/\phi^h\})} dx \\
&= \frac{2}{\pi\phi^h} \int_{\epsilon}^{\infty} \frac{\exp\{x/(2\phi^h)\}}{1 + \exp\{x/\phi^h\}} dx & u = \exp\{x/(2\phi^h)\} \\
&= \frac{4}{\pi} \int_{\epsilon}^{\infty} \frac{1}{1 + u^2} du & 2\phi^h du = \exp\{x/(2\phi^h)\} dx \\
&= \frac{4}{\pi} \arctan(\exp\{x/(2\phi^h)\}) \Big|_{\epsilon}^{\infty} \\
&= 2\left(1 - \frac{2}{\pi} \arctan(\exp\{\epsilon/(2\phi^h)\})\right) \\
&= \frac{4}{\pi} \operatorname{arccotan}(\exp\{\epsilon/(2\phi^h)\}) \\
&\leq \frac{4}{\pi} \operatorname{arccotan}(\exp\{h\}) & \text{if } \epsilon \leq 2h\phi^h
\end{aligned}$$

Since  $0 < \phi < 1$ ,  $2h\phi^h$  converges to 0. Also,  $2h\phi^h \geq 0$  for  $h \geq 0$ . For any  $\epsilon$ , we have  $h'$  that satisfies  $\epsilon \leq 2h\phi^h$  for  $h' \leq h$ . Then, fix such  $h'$ .

$$\begin{aligned}
\int_{h'}^{\infty} \frac{4}{\pi} \operatorname{arccotan}(\exp\{h\}) dh &< \infty \\
\sum_{h=h'}^{\infty} \frac{4}{\pi} \operatorname{arccotan}(\exp\{\epsilon/(2\phi^h)\}) &\leq \sum_{h=h'}^{\infty} \frac{4}{\pi} \operatorname{arccotan}(\exp\{h\}) < \infty
\end{aligned}$$

Therefore,

$$\sum_{h=0}^{\infty} P(|z_h| \geq \epsilon) = \sum_{h=0}^{\infty} \frac{4}{\pi} \operatorname{arccotan}(\exp\{\epsilon/(2\phi^h)\}) < \infty$$

We can also see that when  $|\phi| > 1$ , the sum diverges to  $\infty$ . By Borel-Cantelli lemma, we may conclude that  $\sum_{h=0}^{\infty} z_h$  diverges almost surely.

Define  $y_h = z_h 1_{\{|z_h| \leq \epsilon\}}$ . For the second and the third condition, we need to show that 1)  $\sum_{h=0}^{\infty} E(y_h)$  converges, and 2)  $\sum_{h=0}^{\infty} \text{Var}(y_h)$ , converges. For the second condition, it suffices to show:

$$E\left(\sum_{h=0}^{\infty} y_h\right) = \sum_{h=0}^{\infty} E(y_h) < \infty,$$

which is satisfied by showing  $\sum_{h=0}^{\infty} E(|y_h|) < \infty$  (Fubini). Using Cauchy-Schwartz Inequality:

$$\begin{aligned} \sum_{h=0}^{\infty} E(|y_h|) &= \sum_{h=0}^{\infty} E(|z_h 1_{\{|z_h| \leq \epsilon\}}|) \\ &\leq \sum_{h=0}^{\infty} \sqrt{E(z_h^2) P(|z_h| \leq \epsilon)} \\ &\leq \sum_{h=0}^{\infty} \sqrt{E(z_h^2)} = \sum_{h=0}^{\infty} \sqrt{\text{Var}(z_h)} = \pi \sum_{h=0}^{\infty} \phi^h = \frac{\pi}{(1-\phi)} < \infty. \end{aligned}$$

The second condition is satisfied. For the third condition, similar logic is applied. First note that:

$$\begin{aligned} \text{var}\left(\sum_{h=0}^{\infty} y_h\right) &= E\left(\left(\sum_{h=0}^{\infty} y_h\right)^2\right) + E\left(\left(\sum_{h=0}^{\infty} y_h\right)\right)^2 \\ &= E\left(\left(\sum_{h=0}^{\infty} y_h\right)^2\right) + \left(\left(\sum_{h=0}^{\infty} E(y_h)\right)\right)^2 \\ &= E\left(\left(\sum_{h=0}^{\infty} y_h\right)^2\right). \end{aligned}$$

And,

$$\begin{aligned} \lim_{h \rightarrow \infty} E\left(\left(\sum_{n=0}^h y_n\right)^2\right) &= \lim_{n \rightarrow \infty} E\left(\sum_{h=0}^n y_h^2\right) && \text{(independence)} \\ &= \lim_{n \rightarrow \infty} \sum_{h=0}^n E(y_h^2) = \sum_{h=0}^{\infty} E(z_h^2 1_{\{|z_h| \leq \epsilon\}}) \\ &\leq \sum_{h=0}^{\infty} E(z_h^2) = \frac{\pi^2}{(1-\phi^2)} < \infty \end{aligned}$$

Therefore:

$$var\left(\sum_{h=0}^{\infty} y_h\right) = \sum_{h=0}^{\infty} var(y_h) < \infty$$

All three conditions are satisfied.

## A.2 Theorem 2

When  $\phi = 0.5$ , we have the following special case for the MGF,

$$\begin{aligned} \prod_{h=0}^{\infty} \cos\left(\frac{\pi t}{2^h}\right) &= \prod_{h=0}^{\infty} \frac{\sin\left(\frac{\pi t}{2^{h-1}}\right)}{2\sin\left(\frac{\pi t}{2^h}\right)} = \lim_{n \rightarrow \infty} \prod_{h=0}^n \frac{\sin\left(\frac{\pi t}{2^{h-1}}\right)}{2\sin\left(\frac{\pi t}{2^h}\right)} \\ &= \lim_{n \rightarrow \infty} \frac{\sin(2\pi t)}{2^n \sin\left(\frac{\pi t}{2^n}\right)} = \frac{\sin(2\pi t)}{2\pi t} \end{aligned}$$

We have:

$$\prod_{h=0}^{\infty} \sec\left(\frac{\pi t}{2^h}\right) = \frac{1}{\prod_{h=0}^{\infty} \cos\left(\frac{\pi t}{2^h}\right)} = \frac{2\pi t}{\sin(2\pi t)} = \Gamma(1-2t)\Gamma(1+2t) = \beta(1-2t, 1+2t),$$

where  $\frac{2\pi t}{\sin(2\pi t)} = \Gamma(1-2t)\Gamma(1+2t)$  is by the reflection relation.

Note that the moment generating function (m.g.f) of  $Logistic(\mu, s)$  is  $\exp\{-\mu t\}\beta(1-2t, 1+2t)$ . Since the moment generating function uniquely determines the random variable,

$$z_t = \sum_{h=0}^{\infty} z_{t,h} \xrightarrow{a.s} Logistic(0, 2)$$

Note that

$$f(z_t) = \frac{1}{8} \operatorname{sech}^2\left(\frac{z_t}{4}\right)$$

## A.3 Theorem 3

Let  $\lambda_t := \exp\{v_t\}$ . We showed that  $f(\lambda_t) = \frac{1}{(1+\lambda_t)^2}$ . We have:

$$f(\Delta h_t) = \int_0^{\infty} \frac{1}{\sqrt{2\pi\lambda_t^2}} \exp\left\{-\frac{\Delta^2 h_t}{2\lambda_t^2}\right\} \frac{1}{(1+\lambda_t)^2} d\lambda_t$$

$\forall x > 0$ ,

$$\frac{1}{2(1+x^2)} \leq \frac{1}{(1+x)^2} \leq \frac{1}{(1+x^2)}.$$

Thus,

$$\begin{aligned} f(\Delta h_t) &\leq \int_0^\infty \frac{1}{\sqrt{2\pi\lambda_t^2}} \exp\left\{-\frac{\Delta^2 h_t}{2\lambda_t^2}\right\} \frac{1}{(1+\lambda_t^2)} d\lambda_t \\ &= \frac{1}{2\sqrt{2\pi}} \int_0^\infty \frac{1}{1+u} \exp\left\{-\frac{u\Delta^2 h_t}{2}\right\} du & u = \frac{1}{\lambda_t^2} \\ &= \frac{1}{2\sqrt{2\pi}} \exp\{\Delta^2 h_t/2\} E_1(\Delta^2 h_t/2), \end{aligned}$$

where  $E_1()$  is the exponential integral function, which satisfies the following upper and lower bound  $\forall t > 0$ :

$$\frac{\exp\{-t\}}{2} \log\left(1 + \frac{2}{t}\right) < E_1(t) < \exp\{-t\} \log\left(1 + \frac{1}{t}\right)$$

Thus,

$$f(\Delta h_t) < \frac{1}{2\sqrt{2\pi}} \log\left(1 + \frac{2}{\Delta^2 h_t}\right)$$

Similarly for the lower bound,

$$f(\Delta h_t) > \frac{1}{8\sqrt{2\pi}} \log\left(1 + \frac{4}{\Delta^2 h_t}\right)$$

The lower and upper bound for  $\Delta h_t \neq 0$  is shown. The lower bound clearly approaches infinity as  $\Delta h_t$  approaches 0, which completes the proof.

## B Priors and Full Conditional for Gibbs Sampling

### B.1 Priors

In this section, priors on the parameters  $(\mathbf{h}, \mathbf{v}, \mu, \phi)$  are specified. For computational efficiency, we consider  $\eta_t \sim Z(\frac{1}{2}, \frac{1}{2}, 0, 1)$ . By conditional independence, the prior distribution decomposes as follows:

$$\begin{aligned} f(\mathbf{h}, \mathbf{v}, \mu, \phi) &= f(\mathbf{h}|\mathbf{v}, \mu, \phi) f(\mathbf{v}|\mu, \phi) f(\mu|\phi) f(\phi) \\ &= f(\mathbf{h}|\mathbf{v}) f(\mathbf{v}|\mu, \phi) f(\mu) f(\phi) \end{aligned}$$

In addition to the existing parameters, Four additional parameters  $\mathbf{j} = (j_1, \dots, j_T)', \mathbf{s} = (s_1, \dots, s_T)', \boldsymbol{\xi} = (\xi_1, \dots, \xi_T)',$  and  $\xi_\mu$  are introduced to expand existing parameters. Specifically,  $\forall t$

$$\begin{aligned} f(j_t | y_t^*, h_t) &\propto f(y_t^* | h_t, j_t) f(j_t) \\ f(s_t | \omega_t^*, v_t) &\propto f(\omega_t^* | v_t, s_t) f(s_t) \quad \omega_t^* = \log(\omega_t^2) = \log((h_t - h_{t-1})^2) \\ f(\xi_t | v_t, \mu, \phi) &\propto f(v_t | \mu, \phi, \xi_t) f(\xi_t) \\ f(\xi_\mu | \mu) &\propto f(\mu | \xi_\mu) f(\xi_\mu) \end{aligned}$$

Thus, the parameter expanded priors maybe written as:

$$f(\mathbf{j}, \mathbf{h}, \mathbf{v}, \mathbf{s}, \boldsymbol{\xi}, \mu, \xi_\mu, \phi) = f(\mathbf{j}) f(\mathbf{h} | \mathbf{v}, \mathbf{s}) f(\mathbf{s}) f(\mathbf{v} | \mu, \phi, \boldsymbol{\xi}) f(\boldsymbol{\xi}) f(\mu | \xi_\mu) f(\xi_\mu) f(\phi).$$

In the following, we specify the exact distribution for each conditional prior distributions.

1.  **$f(\mathbf{j})$**  : The prior distribution on  $\mathbf{j}$  is a 10-component Gaussian mixture distribution approximating the log of chi-squared distribution with 1 degree of freedom.
2.  **$f(\mathbf{h} | \mathbf{v}) f(\omega^* | \mathbf{v}, \mathbf{s})$**  : Without any parameter expansion,  $h_t$  depends on its previous  $h_{t-1}$  and its log-variance term  $v_t$ :  $h_{t+1} | h_t \sim N(h_t, \exp\{v_t\})$ . Also, we assume  $f(h_1 | v_1) = \mathcal{N}(h_1 | 0, \exp\{v_1\})$ . Then, we have:

$$f(\mathbf{h} | \mathbf{v}) = \mathcal{N}(h_1 | 0, \exp\{v_1\}) \prod_{t=2}^T \mathcal{N}(h_t | h_{t-1}, \exp\{v_t\})$$

Remember that  $\omega^* := \log(\omega^2) = \log(\Delta \mathbf{h}^2)$ . Thus,  $f(\omega | \mathbf{v}) = \mathcal{N}(0, \exp\{\mathbf{v}\} I)$ . Then,

$$\omega_t^* | v_t = v_t + \lambda_t^* \quad \lambda_t^* \stackrel{iid}{\sim} \log(\chi_1^2)$$

Using the same logic used for the parameter expansion for  $y^*$ , we get

$$f(\omega^* | \mathbf{v}, \mathbf{s}) = \mathcal{N}(\omega^* | \mathbf{v} + \mu_s, I \sigma_s^2),$$

and  $\mathbf{s}$  follows the identical distribution as  $\mathbf{j}$ .

3.  **$f(\mathbf{s})$**  : As explored in the previous item,  $f(\mathbf{s})$  has the identical distribution to  $f(\mathbf{j})$ .

4.  $f(\mathbf{v}|\mu, \phi, \boldsymbol{\xi})$  :  $v_t$  depends on its previous value  $v_{t-1}$ , unconditional mean parameter  $\mu$ , the autoregressive parameter  $\phi$  and the variance term  $\xi_{t-1}$ .  $\eta_t \sim Z(\frac{1}{2}, \frac{1}{2}, 0, 1)$  is a mean-variance mixture of Gaussian distribution with

$$f(\eta_t|\xi_{t-1}) = \mathcal{N}(\eta_t|0, \frac{1}{\xi_{t-1}})$$

$$f(\xi_t) = \mathcal{PG}(\xi_t|1, 0)$$

where PG represents Polya-Gamma random variable. Then, the priors on  $v$  may be expressed as:

$$f(\mathbf{v}|\mu, \phi, \boldsymbol{\xi}) = \mathcal{N}(v_1|\mu, \frac{1}{\xi_0}) \prod_{t=2}^T \mathcal{N}(v_t|\mu + \phi(v_{t-1} - \mu), \frac{1}{\xi_{t-1}}).$$

5.  $f(\boldsymbol{\xi})$  : As shown in item  $v$ , for  $t \in \{0, \dots, T-1\}$

$$f(\xi_t) = \mathcal{PG}(\xi_t|1, 0)$$

6.  $f(\mu|\xi_\mu)$  : For  $\mu$  we have  $m = \sqrt{e^\mu} \sim C^+(\frac{1}{\sqrt{A}})$ , where  $A = 1$ .

$$f(m) = \frac{2\sqrt{A}}{\pi(1+Am^2)} \quad m \geq 0$$

$$f(\mu) = \frac{2\sqrt{A}}{\pi(1+Ae^\mu)} \left| \frac{d}{d\mu} \sqrt{e^\mu} \right| = \frac{\sqrt{Ae^\mu}}{\pi(1+Ae^\mu)} = \frac{\sqrt{e^{\mu-(-\log(A))}}}{\pi(1+e^{\mu-(-\log(A))})} \quad \mu \in (-\infty, \infty)$$

$$= \mathcal{Z}(\mu|\frac{1}{2}, \frac{1}{2}, -\log(A), 1) = \mathcal{Z}(\mu|\frac{1}{2}, \frac{1}{2}, 0, 1).$$

Using the same logic used in item  $f(v|\mu, \phi, \xi)$ , we have

$$f(\mu|\xi_\mu) = \mathcal{N}(\mu|0, \frac{1}{\xi_\mu})$$

$$f(\xi_\mu) = \mathcal{PG}(\xi_\mu|1, 0)$$

7.  $f(\boldsymbol{\xi}_\mu)$  : The parameter  $\xi_\mu$  was introduced to expand the parameter  $\mu$ , which follows a half-Cauchy distribution. As shown in item  $f(\mu|\xi_\mu)$ ,

$$f(\xi_\mu) = \mathcal{PG}(\xi_\mu|1, 0).$$

8.  $f(\phi)$  : Let  $b = \frac{\phi+1}{2}$ .

$$f\left(\frac{\phi+1}{2}\right) = f(b) = Beta(b|10, 2).$$

## B.2 Conditional Distributions for Gibbs Sampling

Based on the likelihood and prior distributions described in the previous sections, conditional posterior distributions for each parameters are explored in this section.

### B.2.1 $j$

$\mathbf{j} = (j_1, \dots, j_T)$  was introduced to expand the likelihood on  $y^*$ . In this section, we show that  $\forall k \in \{1, \dots, 10\}$ :

$$\begin{aligned} p(j_t = k | h_t, v_t, s_t, \xi_t, \mu, \xi_\mu, \phi, y_t^*) &= p(j_t = k | h_t, y_t^*) \\ &= \frac{\mathcal{N}(y_t^* | h_t + \mu_k, \sigma_k^2) p_k}{\sum_{i=1}^{10} p_i \mathcal{N}(y_t^* | h_t + \mu_i, \sigma_i^2)}, \quad \forall t \in \{1, \dots, T\} \end{aligned}$$

$\mathbf{j}$  is only associated with  $y^*$ , which is only associated with  $\mathbf{h}$  and  $\mathbf{j}$ :

$$p(j_t = k | h_t, v_t, s_t, \xi_t, \mu, \xi_\mu, \phi, y_t^*) = p(j_t = k | h_t, y_t^*) = \frac{f(y_t^* | h_t, j_t) p(j_t = k)}{\int f(y_t^* | h, j_t) f(j_t) dj_t}$$

and,

$$f(y_t^* | j_t, h_t) = \mathcal{N}(y_t^* | h_t + \mu_{j_t}, \sigma_{j_t}^2).$$

Naturally,  $\forall k \in \{1, \dots, 10\}$

$$\begin{aligned} p(j_t = k | h_t, y_t^*) &= \frac{f(y_t^* | h_t, j_t = k) p(j_t = k)}{f(y_t^* | h_t)} \\ &= \frac{f(y_t^* | h_t, j_t = k) p(j_t = k)}{\sum_{i=1}^{10} p(j_t = i) f(y_t^* | h_t, j_t = i)} \\ &= \frac{\mathcal{N}(y_t^* | h_t + \mu_k, \sigma_k^2) p_k}{\sum_{i=1}^{10} p_i \mathcal{N}(y_t^* | h_t + \mu_i, \sigma_i^2)}, \quad \forall t \in \{1, \dots, T\}, \end{aligned}$$

which is what we wanted to show. The exact distribution on  $j_t \stackrel{iid}{\sim} Categorical(p_1, \dots, p_{10})$  as well as corresponding mean and the variance parameter of each component is described in ?.

### B.2.2 $h$

In this section, we derive the conditional distribution the state variable  $\mathbf{h}$ :

$$f(\mathbf{h}|\theta_{-h}^{1:T}, \mathbf{y}^*) = f(\mathbf{h}|\mathbf{j}, \mathbf{v}, \mathbf{y}^*) = \mathcal{N}\left(\mathbf{h} \left| \left(Q_v + I \frac{1}{\sigma_j^2}\right)^{-1} \frac{y - \mu_j}{\sigma_j^2}, \left(Q_v + I \frac{1}{\sigma_j^2}\right)^{-1}\right.\right),$$

where  $Q_v$  is a symmetric tridiagonal matrix defined below. Based on section B.1,

$$f(y^*|\mathbf{j}, \mathbf{h}) = \prod_{t=1}^T \mathcal{N}(y_t^*|h_t + \mu_{j_t}, \sigma_{j_t}^2) = \mathcal{N}(y^*|h + \mu_j, I\sigma_j^2)$$

$$f(\mathbf{h}|\mathbf{v}) = \mathcal{N}(h_1|0, \exp\{v_1\}) \prod_{t=1}^T \mathcal{N}(h_t|h_{t-1}, \exp\{v_t\})$$

We derive conditional joint prior on  $h|v$  like we did for  $f(y^*|h, j)$ :

$$\Delta \mathbf{h}|\mathbf{v} = \begin{pmatrix} h_1|v_1 \\ h_2 - h_1|v_2 \\ \vdots \\ h_T - h_{T-1}|v_t \end{pmatrix} \sim N\left(\begin{pmatrix} 0 \\ 0 \\ \vdots \\ 0 \end{pmatrix}, \begin{bmatrix} e^{v_1} & & & \\ & e^{v_2} & & \\ & & \ddots & \\ & & & e^{v_t} \end{bmatrix}\right)$$

Indeed,

$$\mathbf{h}|v \sim \begin{bmatrix} 1 & & & & 0 \\ 1 & 1 & & & \\ 1 & 1 & \ddots & & \\ \vdots & \vdots & \ddots & \ddots & \\ 1 & 1 & \dots & \dots & 1 \end{bmatrix} \Delta h|v \sim N(0, Q_v^{-1})$$

where

$$Q_v^{-1} = \begin{bmatrix} 1 & & & & 0 \\ 1 & 1 & & & \\ 1 & 1 & \ddots & & \\ \vdots & \vdots & \ddots & \ddots & \\ 1 & 1 & \dots & \dots & 1 \end{bmatrix} \begin{bmatrix} e^{v_1} & \dots & \dots & 0 \\ \vdots & e^{v_2} & & \vdots \\ \vdots & & \ddots & \vdots \\ 0 & \dots & \dots & e^{v_t} \end{bmatrix} \begin{bmatrix} 1 & 1 & 1 & \dots & 1 \\ 1 & 1 & 1 & \dots & 1 \\ \ddots & \ddots & \ddots & \ddots & \vdots \\ \ddots & \ddots & \ddots & \ddots & \vdots \\ 0 & & & & 1 \end{bmatrix}$$

And  $Q_v$  is a band matrix

$$Q_v = \begin{bmatrix} \left(\frac{1}{e^{v_2}} + \frac{1}{e^{v_1}}\right) & -\frac{1}{e^{v_2}} & 0 & \dots & \dots & 0 \\ -\frac{1}{e^{v_2}} & \left(\frac{1}{e^{v_3}} + \frac{1}{e^{v_2}}\right) & -\frac{1}{e^{v_3}} & \ddots & \ddots & \vdots \\ 0 & -\frac{1}{e^{v_3}} & \left(\frac{1}{e^{v_4}} + \frac{1}{e^{v_3}}\right) & -\frac{1}{e^{v_4}} & \ddots & \ddots \\ \vdots & \ddots & \ddots & \ddots & \ddots & 0 \\ \vdots & \ddots & \ddots & -\frac{1}{e^{v_{T-1}}} & \left(\frac{1}{e^{v_{T-1}}} + \frac{1}{e^{v_T}}\right) & -\frac{1}{e^{v_T}} \\ 0 & \dots & \dots & 0 & -\frac{1}{e^{v_T}} & \frac{1}{e^{v_T}} \end{bmatrix}$$

We have  $f(\mathbf{h}|\mathbf{v}) = \mathcal{N}(\mathbf{h}|0, Q_v^{-1})$ . Thus, we may conclude that.

$$\begin{aligned} f(\mathbf{h}|\mathbf{j}, \mathbf{v}, y^*) &\propto \mathcal{N}(y^*|\mathbf{h} + \mu_j, I\sigma_j^2) \mathcal{N}(\mathbf{h}|0, Q_v^{-1}) \\ &\propto \mathcal{N}(y^* - \mu_j | \mathbf{h}, I\sigma_j^2) \mathcal{N}(\mathbf{h}|0, Q_v^{-1}). \end{aligned}$$

Posterior on normal likelihood with a known variance and the normal prior on the mean, also known as normal-normal model, has a closed form posterior distribution, which is also Gaussian.

$$f(\mathbf{h}|\mathbf{j}, \mathbf{v}, \mathbf{y}^*) = \mathcal{N}\left(\mathbf{h} \left| \left(Q_v + I \frac{1}{\sigma_j^2}\right)^{-1} \frac{y - \mu_j}{\sigma_j^2}, \left(Q_v + I \frac{1}{\sigma_j^2}\right)^{-1}\right)\right),$$

which is what we wanted to show.

### B.2.3 $v$

In this section, we show that

$$\begin{aligned} f(\mathbf{v}|\theta_{-v}^{1:T}, y^*) &= f(\mathbf{v}|\mathbf{s}, \mathbf{h}, \mu, \phi, \boldsymbol{\xi}) = f(\mathbf{v}|\mathbf{s}, \boldsymbol{\omega}^*, \mu, \phi, \boldsymbol{\xi}) \\ &= \mathcal{N}\left(\mathbf{v} \left| \left(Q_{\xi, \phi} + I \frac{1}{\sigma_s^2}\right)^{-1} \left(\frac{\boldsymbol{\omega}^* - \mu_s}{\sigma_s^2} + Q_{\xi, \phi} \mathbf{1} \mu\right), \left(Q_{\xi, \phi} + I \frac{1}{\sigma_s^2}\right)^{-1}\right)\right) \end{aligned}$$

We use the all-without-loop (AWOL) sampler by ? with parameter expansion on the error term with scale mixture normal distribution.

Let  $\omega_1^* = \log(h_1^2)$  and  $\omega_t^* = \log((h_t - h_{t-1})^2)$ ,  $\forall t \geq 2$ . Since  $h_t - h_{t-1} \sim N(0, e^{v_t})$ ,

$\omega_t^*|v_t = v_t + \lambda_t$ , where  $\lambda_t \stackrel{iid}{\sim} \log(\chi_1^2)$ . Then, without parameter expansion we have:

$$f(\mathbf{v}|\mathbf{h}, \mu, \phi) = f(\mathbf{v}|\boldsymbol{\omega}^*, \mu, \phi) \propto f(\boldsymbol{\omega}^*|\mathbf{v})f(\mathbf{v}|\mu, \phi).$$

Both  $\boldsymbol{\omega}^*|\mathbf{v}$  and  $\mathbf{v}|\mu, \phi$  will be further expanded with variables  $\mathbf{s} = (s_1, \dots, s_T)'$  and  $\boldsymbol{\xi} = (\xi_1, \dots, \xi_T)'$ , respectively for efficient sampling. In the following sections (B.2.3 and B.2.3) we show that:

$$\begin{aligned} f(\boldsymbol{\omega}^*|\mathbf{v}, \mathbf{s}) &= \mathcal{N}(\boldsymbol{\omega}^* - \mu_s|v, I\sigma_s^2) \\ f(\mathbf{v}|\boldsymbol{\xi}, \mu, \phi) &= \mathcal{N}(\mathbf{v}|\mathbf{1}\mu, Q_{\xi, \phi}^{-1}), \end{aligned}$$

which is indeed, the normal-normal model, with the following posterior distribution:

$$f(\mathbf{v}|\mathbf{s}, \boldsymbol{\omega}^*, \mu, \phi, \boldsymbol{\xi}) = \mathcal{N}\left(\mathbf{v} \left| \left(Q_{\xi, \phi} + I\frac{1}{\sigma_s^2}\right)^{-1} \left(\frac{\boldsymbol{\omega}^* - \mu_s}{\sigma_s^2} + Q_{\xi, \phi}\mathbf{1}\mu\right), \left(Q_{\xi, \phi} + I\frac{1}{\sigma_s^2}\right)^{-1}\right)\right),$$

where  $Q_{\xi, \phi}$  is a tridiagonal matrix derived below.

**Parameter expansion:**  $f(\omega^*|v, s)$  Similar to the derivation on the likelihood  $y^*$ , we may approximate  $\log(\chi_1^2)$  with 10-component Gaussian Mixture proposed by ?. Parameter  $\mathbf{s} = (s_1, \dots, s_T)'$  is introduced to expand  $\omega_t^* = \log(\lambda_t^2)$ . (Please refer to section B.1 for more detail.) Then, we get the following parameter expanded conditional prior  $\boldsymbol{\omega}^*|\mathbf{v}, \mathbf{s}$ .

$$\begin{aligned} f(\omega_t^*|v_t) &= \sum_{i=1}^{10} p_i \mathcal{N}(\omega_t^*|\mu_i + v_t, \sigma_i^2) \\ f(\omega_t^*|v_t, s_t = k) &= \mathcal{N}(\omega_t^*|\mu_k + v_t, \sigma_k^2) = \mathcal{N}(\omega_t^* - \mu_k|v_t, \sigma_k^2) \\ f(\boldsymbol{\omega}^*|\mathbf{v}, \mathbf{s}) &= \mathcal{N}(\boldsymbol{\omega}^* - \mu_s|v, I\sigma_s^2) \end{aligned}$$

**Parameter expansion:**  $f(\mathbf{v}|\boldsymbol{\xi}, \mu, \phi)$  Let's now consider the conditional prior on  $\mathbf{v}|\mu, \phi$ . Note that we had  $v_1 = \mu + \eta_0$  and  $\forall t \geq 2, v_t = \mu + \phi(v_{t-1} - \mu) + \eta_{t-1}$ , where  $\eta_t \sim Z(\frac{1}{2}, \frac{1}{2}, 0, 1)$ , with

$$f(\mathbf{v}|\mu, \phi) = \mathcal{Z}(v_1|\frac{1}{2}, \frac{1}{2}, \mu, 1) \prod_{t=2}^T \mathcal{Z}(v_t|\frac{1}{2}, \frac{1}{2}, \mu + \phi(v_{t-1} - \mu), 1).$$

$\boldsymbol{\xi} = (\xi_0, \dots, \xi_{T-1})'$  is introduced to expand  $\mathbf{v}|\mu, \phi$ , particularly the error term  $\eta_t$  such that

$$f(\mathbf{v}|\boldsymbol{\xi}, \mu, \phi) = \mathcal{N}(v_1|\mu, \frac{1}{\xi_0}) \prod_{t=2}^T \mathcal{N}(v_t|\mu + \phi(v_{t-1} - \mu), \frac{1}{\xi_{t-1}}) \\ \xi_t \stackrel{iid}{\sim} PG(1, 0),$$

where PG represents the Polya-Gamma random variable. As an intermediary step, we introduce  $\mathbf{v}^* = (v_1^*, \dots, v_T^*)'$ , where  $v_1^* = v_1$  and  $v_{t+1}^* = v_{t+1} - \phi v_t, t \geq 2$ . This makes  $\mathbf{v}^*$  conditionally independent Gaussian random variables:

$$f(v_1^*|\xi_1, \mu) = f(v_1|\xi_0, \mu) = \mathcal{N}(v_1^*|\mu, \frac{1}{\xi_0}) \\ f(v_t^*|\xi_{t-1}, \mu, \phi) = f(v_t - \phi v_{t-1}|\xi_{t-1}, \mu, \phi) = \mathcal{N}(v_t^*|\mu(1 - \phi), \frac{1}{\xi_{t-1}}) \quad t \geq 2,$$

which can be expressed as multivariate Gaussian:

$$\mathbf{v}^*|\boldsymbol{\xi}, \mu, \phi \sim N\left(\begin{pmatrix} \mu \\ \mu(1 - \phi) \\ \vdots \\ \mu(1 - \phi) \end{pmatrix}, \begin{bmatrix} \frac{1}{\xi_0} & & & \\ & \frac{1}{\xi_1} & & \\ & & \ddots & \\ & & & \frac{1}{\xi_{T-1}} \end{bmatrix}\right).$$

Similar to the derivation for  $h|v$  in section B.2.2, we have:

$$v|\xi, \mu, \phi = \begin{bmatrix} 1 & & & & 0 \\ \phi & 1 & & & \\ \phi^2 & \phi & \ddots & & \\ \vdots & \vdots & \ddots & \ddots & \\ \phi^{T-1} & \phi^{T-2} & \dots & \dots & 1 \end{bmatrix} v^*|\xi, \mu, \phi$$

And  $Q_{\xi, \phi}$  is also a band matrix

$$Q_{\xi, \phi} = \begin{bmatrix} \xi_1 + \phi^2 \xi_2 & -\phi \xi_2 & 0 & \dots & \dots & 0 \\ -\phi \xi_2 & \xi_2 + \phi^2 \xi_3 & -\phi \xi_3 & \ddots & \ddots & \vdots \\ 0 & -\phi \xi_3 & \xi_3 + \phi^2 \xi_4 & -\phi \xi_4 & \ddots & \vdots \\ \vdots & \ddots & \ddots & \ddots & \ddots & 0 \\ \vdots & \ddots & \ddots & -\phi \xi_{T-1} & \xi_{T-1} + \phi^2 \xi_T & -\phi \xi_T \\ 0 & \dots & \dots & 0 & -\phi \xi_T & \xi_T \end{bmatrix}$$

Thus, we get

$$f(\mathbf{v}|\boldsymbol{\xi}, \mu, \phi) = \mathcal{N}(v|\mathbf{1}\mu, Q_{\xi, \phi}^{-1}).$$

#### B.2.4 $s$

In section B.2.2,  $\mathbf{s} = (s_1, \dots, s_T)'$  was introduced to expand  $\boldsymbol{\omega}^*|\mathbf{v}$ . Based on the same argument used in section B.2.1,  $\forall k \in \{1, \dots, 10\}$

$$\begin{aligned} p(s_t = k|\omega_t^*, v_t) &= \frac{f(\omega_t^*|v_t, s_t = k)p(s_t = k)}{\sum_{i=1}^{10} f(\omega_t^*|v_t, s_t = i)p(s_t = i)} \\ &= \frac{\mathcal{N}(\omega_t^*|v_t + \mu_k, \sigma_k^2)p_k}{\sum_{i=1}^{10} p_i \mathcal{N}(\omega_t^*|v_t + \mu_i, \sigma_i^2)}, \quad \forall t \in \{1, \dots, T\}, \end{aligned}$$

$\forall k \in \{1, \dots, 10\}$ ,  $(p_k, \mu_k, \sigma_k^2)$  can be found in ?.

#### B.2.5 $\xi$

In section B.2.3,  $\boldsymbol{\xi} = (\xi_0, \dots, \xi_{T-1})'$  were introduced to expand  $\mathbf{v}|\mu, \phi$ . As shown in ?, given  $\boldsymbol{\eta}|\boldsymbol{\xi} \sim N(0, \frac{1}{\xi})$  and  $\boldsymbol{\xi} \sim PG(1, 0)$ , we have  $\boldsymbol{\xi}|\boldsymbol{\eta} \sim PG(1, \boldsymbol{\eta})$ . As explored in Section B.1:

$$\begin{aligned} v_1 &= \mu + \eta_0 \\ v_t &= \mu + \phi(v_{t-1} - \mu) + \eta_{t-1}, \quad \forall t \geq 2. \end{aligned}$$

Naturally,  $\eta_1 = v_1 - \mu$  and  $\eta_t = v_{t+1} - \phi v_t - \mu(1 - \phi)$ ,  $\forall t \geq 2$ .

$$\begin{aligned} f(\xi_0|\mathbf{v}, \mu, \phi) &= \mathcal{P}\mathcal{G}(\xi_0|1, v_1 - \mu) \\ f(\xi_{t-1}|\mathbf{v}, \mu, \phi) &= \mathcal{P}\mathcal{G}(\xi_{t-1}|1, v_t - \phi v_{t-1} - \mu(1 - \phi)) \quad \forall t \geq 2, \end{aligned}$$

where  $\mathcal{PG}$  represents the density function for Polya-Gamma random variable.

### B.2.6 $\mu$

In this section, we show that:

$$\begin{aligned} f(\mu | \mathbf{v}, \boldsymbol{\xi}, \xi_\mu, \phi) &= f(\mu | \hat{v}_\phi^*, \boldsymbol{\xi}, \xi_\mu, \phi) \propto f(\hat{v}_\phi^* | \mu, \phi, \boldsymbol{\xi}) f(\mu | \xi_\mu) \\ &= \mathcal{N}\left(\mu \left| \left(\frac{1}{\sigma_{\xi,\phi}^2} + \xi_\mu\right)^{-1} \frac{\hat{v}_\phi^*}{\sigma_{\xi,\phi}^2}, \left(\frac{1}{\sigma_{\xi,\phi}^2} + \xi_\mu\right)^{-1}\right)\right), \end{aligned}$$

where  $\hat{v}_\phi^*$  is defined below.

In section B.2.3, we defined  $v^*$  and showed that

$$\mathbf{v}^* | \boldsymbol{\xi}, \mu, \phi \sim N\left(\begin{pmatrix} \mu \\ \mu(1-\phi) \\ \vdots \\ \mu(1-\phi) \end{pmatrix}, \begin{bmatrix} \frac{1}{\xi_1} & & & \\ & \frac{1}{\xi_2} & & \\ & & \ddots & \\ & & & \frac{1}{\xi_T} \end{bmatrix}\right).$$

Let's further transform the parameter  $\mathbf{v}^*$  and define  $v_\phi^*$

$$v_\phi^* | \boldsymbol{\xi}, \mu, \phi = \begin{pmatrix} v_1^* \\ \frac{v_2^*}{(1-\phi)} \\ \vdots \\ \frac{v_T^*}{(1-\phi)} \end{pmatrix} \sim N\left(\begin{pmatrix} \mu \\ \mu \\ \vdots \\ \mu \end{pmatrix}, \begin{bmatrix} \frac{1}{\xi_0} & & & \\ & \frac{1}{(1-\phi)^2 \xi_1} & & \\ & & \ddots & \\ & & & \frac{1}{(1-\phi)^2 \xi_{T-1}} \end{bmatrix}\right),$$

Then, we can see that

$$\begin{aligned} \hat{v}_\phi^* | \boldsymbol{\xi}, \mu, \phi &:= \frac{1}{T} \sum_{t=1}^T v_{\phi,t}^* \sim N(\mu, \sigma_{\xi,\phi}^2) \\ \sigma_{\xi,\phi}^2 &:= \frac{1}{T^2} \left( \frac{1}{\xi_0} + \frac{1}{(1-\phi)^2} \sum_{t=1}^{T-1} \frac{1}{\xi_t} \right) \end{aligned}$$

Let's then consider  $f(\mu|\xi_\mu)$ . Based on section B.1, we showed that  $\mu \sim Z(\frac{1}{2}, \frac{1}{2}, 0, 1)$ . Similar to the parameter  $\xi$  for  $\mathbf{h}$  in section B.2.3, we introduce a parameter  $\xi_\mu$ , so that

$$f(\mu|\xi_\mu) = \mathcal{N}(\mu|0, \frac{1}{\xi_\mu})$$

$$f(\xi_\mu) = \mathcal{PG}(\xi_\mu|1, 0).$$

Clearly, we have the normal-normal model. We conclude

$$\begin{aligned} f(\hat{v}_\phi^*|\boldsymbol{\xi}, \mu, \phi) &= \mathcal{N}(\hat{v}_\phi^*|\mu, \sigma_{\xi, \phi}^2) \\ f(\mu|\xi_\mu) &= \mathcal{N}(\mu|0, \frac{1}{\xi_\mu}) \\ f(\mu|\hat{v}_\phi^*, \boldsymbol{\xi}, \xi_\mu, \phi) &= \mathcal{N}\left(\mu \left| \left(\frac{1}{\sigma_{\xi, \phi}^2} + \xi_\mu\right)^{-1} \frac{\hat{v}_\phi^*}{\sigma_{\xi, \phi}^2}, \left(\frac{1}{\sigma_{\xi, \phi}^2} + \xi_\mu\right)^{-1}\right)\right). \end{aligned}$$

### B.2.7 $\xi_\mu$

Note that  $\xi_\mu$  only depend on  $\mu$ , where prior on  $\mu|\xi_\mu \sim N(0, \frac{1}{\xi_\mu})$ . Using the same derivation for  $\xi|v, \mu, \phi$  in section B.2.5, we have:

$$f(\xi_\mu|\mu) = \mathcal{PG}(\xi_\mu|1, \mu)$$

### B.2.8 $\phi$

For the parameter  $\phi$ , we have

$$f(\phi|v, \boldsymbol{\xi}, \mu) = f(\phi|\hat{v}_\mu, \boldsymbol{\xi}, \mu) \propto f(\hat{v}_\mu|\boldsymbol{\xi}, \mu, \phi) f(\phi)$$

Let's remind ourselves that  $t \geq 2$ ,  $v_t = \mu + \phi(v_{t-1} - \mu) + \eta_{t-1}$ , and with parameter expansion on  $\eta_t$ , we have

$$f(v_t|v_{t-1}, \mu, \xi_t) = \mathcal{N}(v_t|\mu + \phi(v_{t-1} - \mu), \frac{1}{\xi_{t-1}})$$

$t \geq 2$ , let's define:

$$v_{\mu,t} = \frac{1}{2} \left( \frac{v_t - \mu}{v_{t-1} - \mu} + 1 \right)$$

$$\hat{v}_\mu = \frac{1}{T-1} \sum_{t=2}^T v_{\mu,t}$$

Then, we have:

$$f(v_{\mu,t} | \mu, \xi_{t-1}) = \mathcal{N} \left( \frac{1}{2} \left( \frac{v_t - \mu}{v_{t-1} - \mu} + 1 \right) \middle| \frac{\phi + 1}{2}, \frac{1}{4\xi_{t-1}(v_{t-1} - \mu)^2} \right) \quad t \geq 2$$

$$f(\hat{v}_\mu | \mu, \xi) = \mathcal{N} \left( \hat{v}_\mu \middle| \frac{\phi + 1}{2}, \frac{1}{(T-1)^2} \sum_{t=2}^T \frac{1}{4\xi_{t-1}(v_{t-1} - \mu)^2} \right)$$

And we have:

$$\frac{\phi + 1}{2} \sim Beta(10, 2)$$

We may think of this as a normal likelihood with the known variance and an unknown mean parameter that follows a Beta distribution. Slice sampling by ? was used to sample from the conditional distribution.

## C Additional Figures

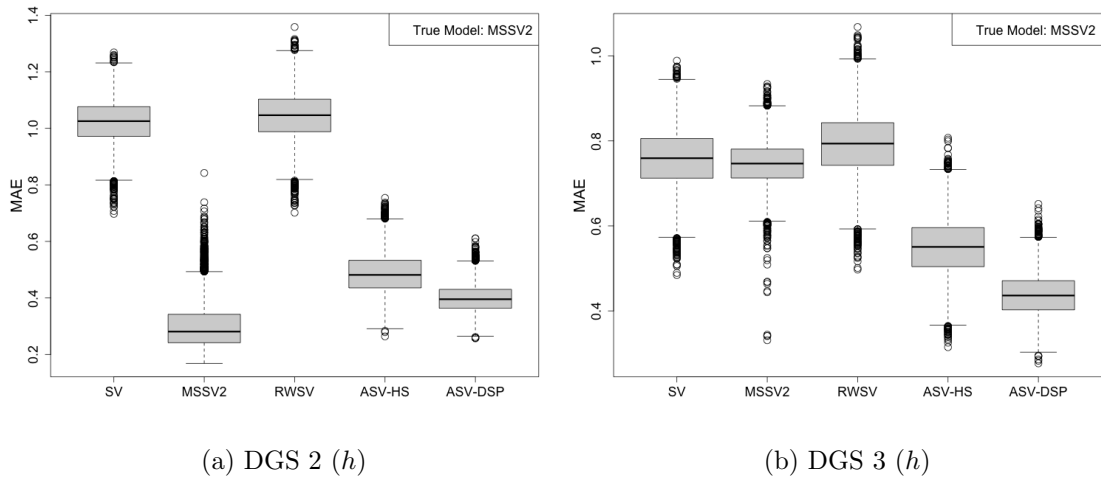


Figure 1: Identical figures to Figure but excluding Random Walk Stochastic Volatility with Bayesian LASSO to allow better comparisons among models. Box plots of Mean Absolute Error (MAE) across 10,000 sample paths measure in  $h$  for Data Generating Scenarios (DGS) 2 and 3. Stochastic Volatility (SV) Markov-Switching Stochastic Volatility with 2 Regimes (MSSV2), Random Walk Stochastic Volatility with Inverse Gamma Prior (RWSV), and Adaptive Stochastic Volatility with Dynamic Horseshoe Prior (ASV-HS), and ASV with Dynamic Shrinkage Processes (ASV-DSP) are compared.